14

Implication of Zeolite Chemistry in Electrochemical Science and Applications of Zeolite-Modified Electrodes

Alain Walcarius
Centre National de la Recherche Scientifique (CNRS)—Université Henri Poincaré (UHP) Nancy I, Villers-lès-Nancy, France

I. INTRODUCTION

The growing interest for zeolite molecular sieves in electrochemistry arises from the synergistic combination of the attractive properties of these materials with electrochemical interfaces. The attractive zeolite characteristics that are liable to affect the electron transfer reactions at an electrode–solution interphase are (a) the size and shape selectivity due to the rigid structure made of pores and channels of molecular dimensions; (b) the cation-exchange capacity arising from the charge compensation of the negatively charged aluminosilicate lattice by mobile extraframework cations; and (c) the catalytic properties of both intrinsic and extrinsic sites of the microporous materials. This has led to the design, preparation, and use of various zeolite-modified electrodes, which form a sub-category of the so-called chemically modified electrodes (CMEs).

The concept of CMEs was introduced by Murray (1). It consists of intelligently designing the surface of conventional electrodes in order to control or to improve their response by combining the intrinsic properties of the modifier to a selected electrochemical reaction. This electrochemist's desire was the starting point of overwhelming developments in the past two decades. Most of the traditional and advanced applications for CMEs are based on the ability of such "integrated chemical systems" to impart both catalytic properties to the electrode surface and to selectively incorporate a target analyte prior to its sensitive electrochemical detection. Electrocatalysis and electroanalysis are two major aims that have driven the fruitful design of CME surfaces (2). The former relies on circumventing the slow heterogeneous reaction kinetics often associated with an electrochemical event by lowering the electron free energy, while the latter is directed to improving both sensitivity and selectivity for a target substrate by exclusive preconcentration at the electrode–solution interface. The efficiency of both of these applications is strongly related to the nature of CMEs, helping to explain the enormous chemical diversity observed in the molecular design of electrode surfaces (3–6).

This chapter will focus primarily on state-of-the-art of CMEs involving zeolites. It includes (a) a description of the various approaches to preparing zeolite-modified electrodes (ZMEs); (b) the effect of confining zeolites at an electrode surface on its response to various electroactive probes; (c) the electrochemistry of zeolites modified with ion-exchanged or encapsulated electroactive guests; (d) the mutual interest between zeolite chemistry and electrochemical science; and (e) numerous advanced applications of ZMEs.

Several reviews have appeared in the literature during the past decade, devoted entirely (7–13) or in part (14–21) to the implication of zeolites in electrochemistry. They illustrate the intense activity in combining zeolite properties with electrode processes. Due to the electronically insulating character of zeolites, their implication in electrochemistry requires close contact to an electronically conducting material. This step in creating an interphase containing an electrode and a zeolite is not trivial (partly because of the powdered form of the aluminosilicate) and various strategies were applied to prepare ZMEs from zeolite particles and conventional electrode materials. The electrochemical behavior of ZMEs depends on (a) the nature of the electroactive guest and the nature and structure of the zeolite host; (b) the type of ZME; (c) the nature and concentration of the so-called supporting electrolyte* (especially the cation size and charge) in the solution surrounding the ZME surface; (d) the location and mobility of the electroactive guest (and other counterions) inside the microporous solid; (e) the time afforded to the ZME to contact the electrolyte solution; (f) the temperature; and (g) the solvent (most electrochemical experiments have been carried out in aqueous medium, although some studies have been done in organic solvents). A fundamental question that arises when combining zeolites and electrochemistry is, when an electroactive guest is initially exchanged or encapsulated within a zeolite particle, according to what pathway(s) do/can charge-transfer reactions occur at ZMEs? Although some controversial discussions have appeared in the literature to support an intracrystalline or an extracrystalline electron transfer mechanism (9,11,22–26), it is now established that the major part of the electrochemical response of ZMEs is due to two main components: extrazeolite electroactive species (always observed with ion exchangeable species, by nature) and/or electroactive species located in or occluded within the cages or channels situated at the boundary of zeolite particles contacting the electrode surface. The relative weight of these two species in the electrochemical response is controlled by the interplay between charge-transfer and mass transport processes occurring at ZMEs, which can be very different depending on various experimental parameters.

In addition to the fascinating fundamental studies aimed at understanding the basic behavior of ZMEs, many advanced applications have been achieved by exploiting the intersection between zeolite chemistry and electrochemical science. These include electrocatalysis directed to sensing or organic synthesis, various aspects of electroanalysis (preconcentration and permselectivity, indirect amperometric detection, potentiometry, biosensors), dispersion electrolysis, solid electrolytes for power sources, photoelectrochem-

* Most electrochemical experiments are performed in solutions containing (in addition to the analyte) a high concentration of inert electrolyte, called supporting electrolyte, in order to minimize the phenomenon of migration of the electroactive ions caused by the electric field. It also confines the interfacial potential difference to the distance of closest approach of solvated ions to the electrode. This has a concentration at least 100 times that of the electroactive analytes and is the principal source of electrically conducting ionic species. At ZMEs, the supporting electrolyte cation plays an important role for charge compensation in zeolites.

istry, as well as the exploitation of the electrochemical techniques to characterize ion-exchange and diffusion processes in zeolites.

II. HISTORICAL ACCOUNT OF ELECTROCHEMISTRY INVOLVING ZEOLITES

The first report using zeolites for electrochemical purposes, dated 1939, has been described by Marshall (27) and involves the potentiometric response of zeolite-containing membrane electrodes to various mono- and divalent cations. This work and some subsequent investigations by the same group (28–31) considered the inorganic membranes as polyelectrolytes with mobile cations, allowing for the characterization of cation activities similar to the way that the glass membrane electrode is used for determining hydrogen ion activities. This pioneering approach was then pursued by Barrer and James (32) in 1960, providing a more quantitative treatment of the zeolite membrane potential and discussing its relation to the selectivity with respect to cation mixtures in solution. Such potentiometric applications exploit the solution-like ionic conduction of zeolites. A few years later, the solid-state ionic conduction of zeolites was utilized in electrochemistry by designing solid-state batteries (33,34) and fuel cells (35,36), with zeolite particles acting as a solid electrolyte and as a host for the catholite (in batteries) or for electroreactants or water (in fuel cells). Finally, at the end of the 1970s, Susic and Petranovic (37–40) investigated the electrochemical behavior of dry zeolite crystals at temperatures above 200°C, where dry zeolite displays solid-state ionic conduction (41). At these high temperatures, the zeolite acted as a "solvent" for the charge-compensating cations that can be reduced on platinum; examples are available for reduction of Na^+ (38), Cd^{2+} (39), and Ag^+ (40). These latter investigations are the first examples of electrodics* involving zeolites, while the above potentiometric experiments were only concerned with ionics.†

Modern fields of investigation concerning the zeolite–electrochemistry intersection began in the 1980s with considerable research on ZMEs since 1988. It is noteworthy that the (often) preliminary works performed in this initial mid 80's period suggested most of the application types as well as electrode configurations. Some milestones are:

- Pereira-Ramos et al. (42,43) prepared zeolite-supported metal catalysts using electrochemical techniques. By means of a pressed composite electrode made of graphite and silver-exchange mordenite particles, they were able to produce electrochemically some clusters of metallic silver within the mordenite particles, and crystallites or dendritic deposits on the graphite particles (43).
- One year later, Murray et al. (44) grew electrogenerated coatings comprising zeolites; this was achieved by continuous potential cycling at a rotated disk electrode (Pt or C) in an organic solvent containing fine zeolite particles in suspension and an appropriate soluble electroreactant.
- Concurrent and competing with this approach is the evaporative deposition of a zeolite-polystyrene composite layer on solid electrode surfaces, which is carried

* The term electrodics concerns the part of electrochemistry that involves the study of processes in which transfer of an electron occurs across an electrochemical interface, often made between an electrode and an ionically conducting medium.

† The term ionics is related to the part of electrochemistry devoted to the study of only the ionically conducting phases (without any associated electron transfer reaction).

out with suspensions of powdered zeolite in polymer solutions, as first described by de Vismes et al. (45). They have also incorporated some metal porphyrins into the ZME and explored their electrocatalytic properties; in this case, the zeolite is thought to enhance the chemical stability of the catalyst.

- Hernandez et al. (46) described the first zeolite-modified carbon paste electrode, by mixing graphite particles with a natural zeolite from the Canary Islands and a mineral oil binder, and applied it to the voltammetric analysis of Hg^{II} after chemical accumulation by ion exchange within the zeolite.
- Finally, the group of Shaw (47,48) initiated what has become one of the largest challenges of ZME electrochemistry: (a) to determine and, if possible, control the factors affecting the behavior of ZMEs; and (b) to understand the origin of the electrochemical response of ZMEs by proposing mechanistic models for charge transfer.

At the end of the 1980s, the two main methods for preparing ZMEs were zeolite overlayers on solid electrodes and zeolite dispersions into a composite electrode material. Subsequent efforts were often directed to optimizing these generic procedures to get longer durability and better electrochemical perspectives, rather than evaluating totally new directions (e.g., in situ grown zeolite films on conducting substrates like gold or mercury (49–51). An exception is the unconfined metal-doped zeolite dispersions used by Rolison et al. (52,53) as electrode-modified zeolites. The main applications predicted during this startup period, including electrocatalysis and several aspects of electroanalysis and sensors, were largely developed during the last decade of the 20th century. One should also mention that the field of energy storage that exploits the adsorbent properties of zeolites was still growing in the 1980s, especially prompted by Coetzer (54,55), and that the use of zeolites as solid electrolytes in batteries remains common.

III. DESIGN AND PREPARATION OF ZEOLITE MODIFIED ELECTRODES

Starting an electrochemical study with electronically insulating zeolite particles implies confining them at an electrode surface. This construction step should be reasonably easy and should provide ZMEs with good conductivity properties (low resistance and low capacitance), high mechanical stability and long-term durability, as well as reproducible characteristics (for both their fabrication procedures and their electrochemical responses). Of course, such ideal conditions leading to high-quality chemically modified electrodes that would display adequate electrochemical signals (3,6) are not easily fulfilled when zeolite is used as the electrode modifier. This is because its insulating character will lower the electrode conductivity, and individual solid crystals of micrometer dimension and rigid structure will result in heterogeneous composition and configuration of the modified electrode material. This in turn could impart rather low mechanical stability in stirred media due to possible leaching of zeolite particles into the solution. These are some of the reasons why many efforts have been directed to finding the best strategies to prepare ZMEs, as illustrated in Table 1. The corresponding references are provided to give a rapid view on the most widely used electrode configurations, as well as experimental details required to build a particular ZME. In spite of the aforementioned difficulties, several ZMEs with satisfactory characteristics have been obtained, with electrode design being most often dictated by the target application.

Table 1 shows that most ZMEs are prepared according to two main methods: (a) zeolite-polymer films coated on solid electrode surfaces and (b) bulky zeolite-carbon or zeolite-carbon-binder composites or, alternatively, a combination of these two generic

Table 1 Main Reported Methods for Use of Zeolites in Electrochemistry and Design of Zeolite-Modified Electrodes

Various types of zeolite-modified electrodes	Ref.
A. Zeolite coatings on conventional electrode substrates	
A1. Evaporation of zeolite-polymer suspensions	
Zeolite-polystyrene composite films	45, 47, 48, 56–64, 66, 67, 69, 82, 83
Other zeolite-polymer films	75, 77, 80, 81, 85
Zeolite-carbon-polystyrene composite films	94, 104–108
Screen-printed zeolite-carbon composite films	170, 177
A2. Deposition of zeolite mono- or multilayers	
Dense zeolite monograin layer (covered by a thin polystyrene film)	65, 68, 70–72, 74
Dense zeolite multilayers (covered by a thin polymer film)	73, 76, 78, 79, 84, 86–88, 89, 191
Dense zeolite-carbon layers (covered by a thin polymer film)	24, 109
Thin zeolite films grown on conducting surfaces	110, 111
A3. Other chemical or physicolchemical deposition processes	
Coelectrodeposition from a mixture containing zeolites and organic species	8, 44, 95
Electropolymerization of an organic monomer in the presence of zeolite	7, 95–98
Photopolymerization of ethylene-linked zeolite particles	90
Electrophoretic deposition	91–93
B. Zeolite particles dispersed in the bulk of a composite material	
B1. Dispersion into a conducting composite matrix	
Zeolite-modified carbon paste electrodes	46, 48, 73, 84, 146–173
Zeolite-carbon-copolymer composites	174–176
B2. Dispersion into a nonconducting matrix	
Zeolite-polymer membranes	27–32, 99–103
C. Others	
C1. Pressed or compacted zeolite particles	
Zeolite + carbon mixtures pressed on a metallic grid	20, 25, 43, 45, 112–128
Zeolite + carbon pellets	152
Zeolite alone:	
- pressed pellets or compacted disks contacting an electrode	143, 187
- zeolite particles pressed between two electrode feeders	37–40, 129–131
Zeolite-based solid electrolytes	33, 34, 132–142
C2. Covalent linkage of zeolite particles to a solid electrode surface	
Zeolite attached to SnO_2 via a silane coupling agent	178
C3. Unconfined zeolites	
Zeolite dispersion and slurries	52, 53, 109, 179–186

approaches. The various ZME designs obtained from these basic configurations are briefly described hereafter, wth special emphasis on their advantages and limitations. Most of them have been discussed in the literature (9,11).

A classical route to chemically modify an electrode surface is to cover it by an adhesive layer of the modifying agent. This simple approach was successfully applied to polymer modified electrodes, but it is prevented here as the zeolite particles do not stick by themselves to the surface of conventional electrodes. Cohesion would require a binder. This is what has motivated the development of zeolite-polymer films coated on solid electrode surfaces.

Several cases have been reported and are schematically illustrated in Fig. 1. A composite zeolite-polymer film can be easily deposited on a solid electrode by evaporation of an organic solution containing a dissolved polymer (mainly polystyrene) and suspended zeolite particles. This rather simple procedure has been widely used (45,47,48,56–89) and gives rise to porous films that enable diffusion processes to occur at the electrode–film–solution interfaces by way of the free space ("void") remaining in the composite after solvent evaporation. Such films are, however, somewhat heterogeneous because of the usually weak zeolite–polymer interactions (while the polymer often adheres strongly to the electrode surface) (48) and must be used only in unstirred solutions to avoid leaching of zeolite particles into solution. A modified approach is to deposit first a pure zeolite layer on the electrode surface and then to cover it with a thin porous polymer film to ensure mechanical stability. Two configurations are possible: (a) the dense monograin layer

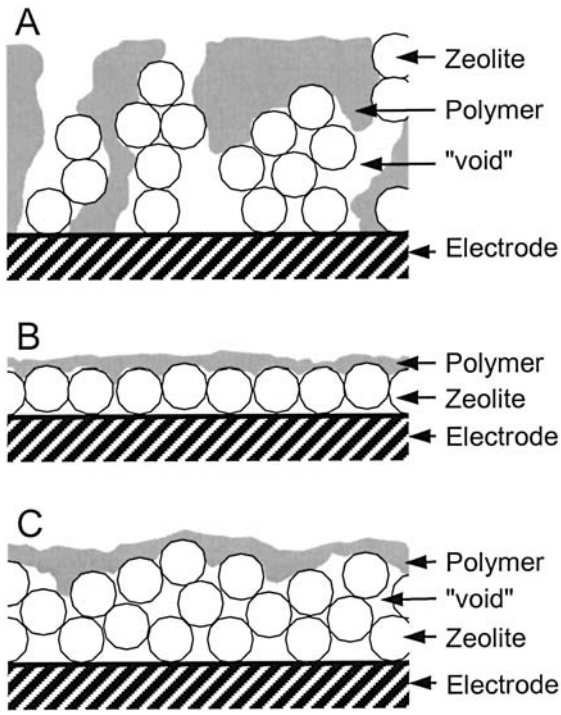

Fig. 1 Schematic representation of zeolite-polymer film–based ZMEs. (A) Zeolite-polymer film obtained by evaporation of zeolite particles suspended in a polymer solution; (B) zeolite monograin layer covered with a thin polymer film; (C) zeolite multilayer covered with a thin polymer film.

introduced by Calzaferri's group (74,90), which requires zeolite particles of monodisperse size; and (b) the dense zeolite multilayer (73,76) that does not require absolutely homogeneous morphologies and sizes of the zeolite particles. This last design results in small "void" spaces in the zeolite layer because of a random distribution of particles, whose packing can be improved by electrophoretic deposition of zeolites that leads to more mechanical stability (91–93). These dense films are claimed to be robust enough to be used in a stirred medium (11). Though sometimes used in nonaqueous media (47,63,94), the zeolite-polymer films are more stable in aqueous solutions because of possible (fortunately slow) dissolution of the polymer binder in organic solvents.

Alternative methods to produce films comprising zeolite particles in an organic binder were also suggested. Zeolite can be embedded into an organic matrix during its formation by electrodeposition, i.e., reduction of 1,4-dinitrobenzene (8,44) or reduction of phenosafranine (95) on carbon electrodes. Composite films made of zeolite dispersed into an electrogenerated conducting polymer were synthesized by electropolymerization of a monomer solution containing zeolite particles in suspension (96–98). This led to zeolite-polymer composites of better conductivity than the corresponding zeolite-polystyrene coatings. One should also mention the nonconducting zeolite-polymer membranes made of a zeolite dispersion within an inert organic resin (27,32,99–103), which are suited for potentiometric measurements via exploitation of the ionic conduction of zeolites.

Another way to improve the conductivity of ZMEs made of two resistive elements (i.e., polystyrene and zeolite) is to add carbon powder to the film. This is readily achieved by grinding together carbon and zeolite particles prior to dispersing them in the polymeric binder (94,104–106). Coating of such zeolite-carbon-polymer films on ultramicroelectrodes (10 μm diameter) was reported (107,108). Carbon was also used to increase the area of electrical conductor in direct contact to the zeolite in dense films covered by a thin polystyrene overlayer (24,109). If resistance of these films was indeed lowered as compared with that of carbon-free coatings, it should be emphasized that capacitance of the ZME was also significantly increased due to a much higher area of the electrode surface. Thin zeolite films grown on conducting surfaces are also reported (110,111).

Thin zeolite-carbon pellets were prepared for electrochemical purposes by pressing a dry graphite-zeolite mixture on a stainless steel grid, resulting in the binder-free ZME schematically depicted in Fig. 2. This electrode configuration characterized by the absence of any organic binder was largely used by Bedioui's group for investigations in nonaqueous media (20,25,43,45,112–128). It was proven that no significant loss in the crystal structure of the molecular sieve occurred during pelletization. Such a ZME made of only zeolite and carbon prevents complications arising from side reactions with a binder and allows the external solution to swell the entire volume of the electrode so that the entire zeolite content is thought to participate to the electrochemical event (11). Its main drawback is low mechanical stability, which leads to crumbly behavior in stirred solution.

Compacted zeolite without graphite has been used to produce ZME devices that exploit the solid electrolyte properties of the molecular sieve material. Zeolite pellets were inserted between two platinum electrodes and the resulting system was placed in a furnace to facilitate study of the electrochemistry of zeolites above 200°C (38–40,129–131). Zeolite particles were also compacted between two current collectors when used as solid electrolytes in batteries (33,34,132–142). Finally, the mechanical contact between an electrode material and a zeolite pellet can be achieved by chemical deposition of a metal coating (e.g., gold) on a zeolite disk (143).

The most widely used method to prepare ZMEs is the incorporation of zeolite particles into the bulk of a so-called carbon paste (Table 1). Carbon paste was invented a

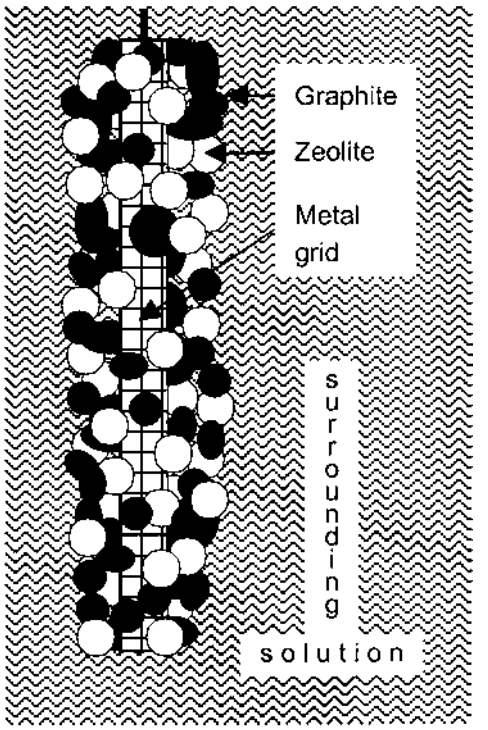

Fig. 2 Schematic representation of a ZME made of a "zeolite + carbon" mixture pressed on a metallic grid.

long time ago and consists of a homogeneous mixture of carbon powder and pasting liquid (144). This matrix has taken a prominent position in the development of chemically modified electrodes because of its good electrochemical characteristics and its simple modification by a large variety of chemicals and biochemicals (145). It is therefore not surprising that many investigations on ZMEs were carried out using zeolite-modified carbon paste electrodes (ZMCPEs) (46,48,73,84,146–173), with a simplified view given in Fig. 3. Their surfaces can be renewed by simple mechanical smoothing, which constitutes a definite advantage over film-based ZMEs that would require the fabrication of a new electrode between each measurement (at least if chemical regeneration cannot be applied). However, the high reproducibility of the mechanical renewing of ZMCPE requires a homogeneous composition of the zeolite-modified paste (not so easily obtained). In principle, only the zeolite particles located at the electrode–solution interface should be involved in the electrochemical processes because they are the only ones in contact with the electrolyte solution. In practice, however, the hydrophilic character of zeolite particles and the imperfect compaction of the composite allow the surrounding solution to enter progressively micrometer thick regions of the paste, more deeply the longer the electrode is exposed to the aqueous solution (150). This limits some practical applications of ZMCPEs from memory effects arising from analytes remaining inside the electrode between successive measurements.

An alternative to ZMCPE is the zeolite-modified carbon-polystyrene-divinylbenzene composite electrodes proposed by Shaw and Creasy (174–176). This composite is by far

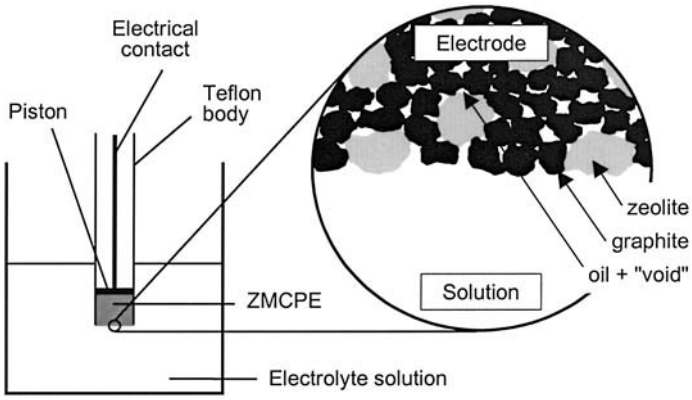

Fig. 3 Schematic representation of the zeolite-modified carbon paste electrode, with an exploded view of the electrode–solution interface.

more robust than carbon paste and can also be renewed by simple mechanical smoothing. No diffusion of the external solution in the bulk of the electrode was reported, but the existence of some remaining micro- or nanocracks (formed during the copolymer synthesis) can lead to some memory effects that cannot be eliminated by the simple mechanical smoothing step.

A more recent approach to zeolite-carbon-polymer composites exploits screen–printing technology to prepare single-use ZMEs (170,177). The process consists of dispersion of zeolite particles into carbon ink, which is subsequently deposited on a ceramic substrate. After solvent evaporation, one obtains a thick (≈ 200 μm) composite film containing zeolite particles embedded in a carbon-polymer matrix. This kind of ZME can be manufactured in series and is therefore promising for routine analysis purposes.

Finally, one should mention original work by Li et al. (178) who have been able to confine zeolite Y particles on an SnO_2 electrode surface by covalent linkage. This was achieved by using the following silane coupling agent:

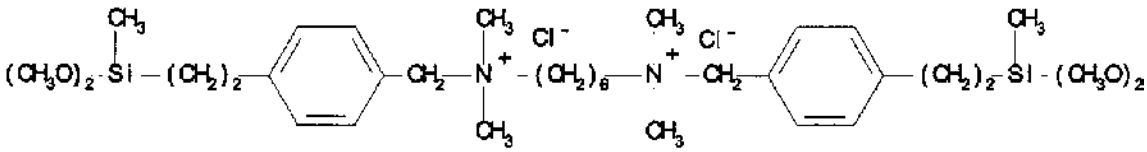

which can react with both the SnO_2 and zeolite surfaces to give a mechanically stable zeolite layer on the electrode surface. This particular spatial arrangement has allowed building of trimolecular redox chains at ZME.

In addition to all of these examples of ZMEs with zeolite particles confined at an electrode surface, another way to intersect zeolite chemistry with electrochemical science was initiated and largely developed by Rolison and coworkers (13,52,53,109,179–186), who introduced the concept of electrode-modified zeolites (52,53). It consists of dispersing zeolite-supported catalysts (often metal micro- and nanostructures in and on zeolite particles) by gas flow into electroreactors made of two feeder electrodes on the cell walls (Fig. 4). The metal nanostructures then act as zeolite-supported ultramicroelectrodes (52).

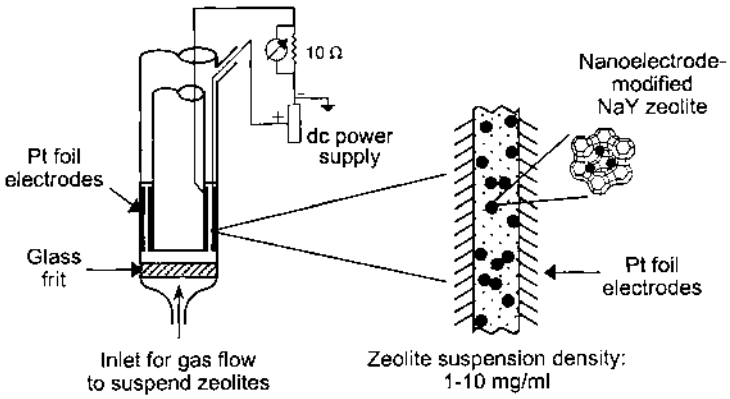

Fig. 4 Schematic representation of electrode-modified zeolites. Dispersion electrolysis cell showing the electrode particles contained between feeder electrodes with an exploded view of intra/extracrystalline Pt supported on zeolite Y. (Reprinted with permission from Ref. 13.)

IV. ELECTROCHEMICAL RESPONSE OF ZEOLITE-MODIFIED ELECTRODES

A. Factors Affecting the Electrochemical Activity of Electroactive Species at ZMEs

1. Concentration of Solution Phase Electroactive Probes at the ZME Surface

When immersing ZME into an electrolyte solution containing a positively charged electroactive probe liable to be accumulated within the zeolite, the electrochemical response of the electrode is more intense than recorded on a corresponding unmodified electrode (48,73). This is illustrated in Fig. 5* for the analysis of $Ru(NH_3)_6^{3+}$ at a platinum electrode coated with a film of zeolite NaY, where the voltammetric peak currents were much larger than those sampled with using unmodified Pt. The increase in sensitivity is explained by the $Ru(NH_3)_6^{3+}/Na^+$ exchange in the zeolite particles, which increases the local concentration of the electroactive cations at the electrode–solution interface. It should be highlighted that the concentration effect must be very important to observe significant increase in peak currents,† since diffusion processes inside the restricted porous structure of zeolites are always much slower than in solution (41).

---

* All voltammograms depicted in this chapter are presented according to the IUPAC convention, with anodic currents on the upper part of the curve and the cathodic component below (note that the current on the anode is considered a positive current according to international convention; however, in electroanalytical chemistry the anodic current is often considered negative; and inversely for the cathode).

† Peak currents observed in voltammetry are often limited by diffusion of electroactive species to the electrode surface. Under these conditions, at a constant scan rate, they are proportional to the product $C \times D$, where C represents the analyte concentration and D its diffusion coefficient. If concentration of electroactive species in the soaking solution and zeolite film is given by C_s and C_f, respectively, with corresponding diffusion coefficients, D_s and D_f, the equality $C_f \times D_f^{1/2} = C_s \times D_s^{1/2}$ corresponds to the same contribution of both solution phase and zeolite phase electroactive probes to the peak current (i.e., a current response at ZME twice as intense as that obtained without zeolite, which is almost the case in Fig. 5). As the term D_f is always much smaller than D_s, the effective electroactive concentration in the zeolite film must be significantly larger than that in solution.

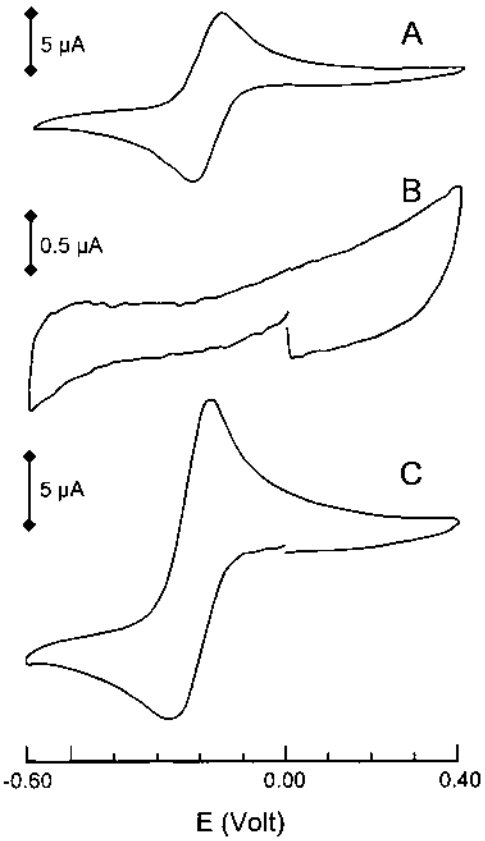

Fig. 5 Cyclic voltammograms using SCE reference electrode. (A) Uncoated platinum electrode in 1 mM $Ru(NH_3)_6^{3+}$ and 0.1 M KNO_3; (B) same platinum electrode as in (A) coated with zeolite NaY, in 0.1 M KNO_3 solution in the absence of $Ru(NH_3)_6^{3+}$; (C) same electrode coated as in (B) 2 h after addition of 1 mM $Ru(NH_3)_6^{3+}$. (Reprinted with permission from Ref. 48.)

Performance of ZME is quantified by defining an enhancement factor as the ratio of peak current density observed at a ZME to that at a corresponding unmodified electrode (48). An enhancement factor higher than one is related to an effective concentration effect whereas values lower than 1 reveal the exclusion of the electroactive probe from the zeolite or a screening behavior of the zeolite layer with respect to species in solution (only for film-based ZME). This quantitative parameter is dependent on various experimental factors: the zeolite type and particle size, the nature and concentration of the electroactive probe, the ZME configuration, and the time afforded to the ZME to soak in the analyte solution (73). Data are available in the literature for several analytes [Ag^+, Cu^{2+}, Pb^{2+}, Cd^{2+}, $Ru(NH_3)_6^{3+}$, $Fe(CN)_6^{3-}$, methyl and heptyl viologen, dopamine, molecular oxygen], three zeolites (A, X, Y), and three electrode configurations (zeolite-modified carbon paste, zeolite-carbon-copolymer composite, zeolite film on glassy carbon) (47,48,73,93,175,151). Some conclusions are briefly summarized here. The enhancement factors calculated from cyclic voltammetry experiments were highest for cationic analytes displaying the highest positive charge and the smallest size, and for zeolites of highest ion-exchange capacity, largest pore size, and smallest particle size. All of these optimal parameters lead to fast transport of the electroactive species at the electrode–solution interface, which constitutes

the rate-determining process when ZMEs are used in the preconcentration-voltammetric detection scheme. Peak heights were also found to increase by increasing the duration of ZME exposure to the solution prior to electrochemical analysis because longer soaking times resulted in a larger amount of electroactive cations exchanged in zeolites. Peak currents recorded as a function of time leveled off more quickly for higher analyte concentrations. On the other hand, the lower the analyte concentration, more efficient the preconcentration, especially when the zeolite exhibits significant preference for the electroactive cation over the electrolyte cation (e.g., in the case of ion-exchange isotherms dictating equivalent fractions of the electroactive cation higher in the zeolite than in solution). In general, bulk zeolite–modified electrodes gave faster enhancement behavior compared to zeolite film–based electrodes. This is because zeolite particles are in direct contact with the electroactive analyte in the former case upon immersion of the electrode into solution, whereas reaching the zeolite layer might be delayed in the latter case due to the hydrophobic character of the polymer binder (or overlayer). Among the bulk zeolite-carbon-based materials, the zeolite-carbon-polystyrene-divinylbenzene and the screen-printed zeolite-carbon composites usually gave better performance than the zeolite-modified carbon paste electrodes (170,175). Depending on the above-mentioned parameters, the observed experimental enhancement factors ranged between 1 and 10 for various analytes, with the exception of silver(I) for which values as high as 40 were obtained after 15 min exposure to a 1 mM Ag^+ solution (73). Size-excluded electroactive cations (those of size larger than the zeolite pore aperture) and charge-excluded species (anions) did not result in any enhancement of the voltammetric peaks.

The approaches just described aim to investigate the behavior of ZMEs with respect to solution phase electroactive probes. However, much of the work on ZMEs, has been performed with electrode systems made of zeolites previously loaded with an electroactive species. A major distinction has to be made between species incorporated in zeolites by ion exchange, which are therefore liable to undergo back exchange when soaking ZME into an electrolyte solution, and species encapsulated in a zeolite host as "ship-in-a-bottle" complexes that have restricted freedom of movement inside the molecular sieve.

2. Electrochemical Activity of Electroactive Species Ion Exchanged in Zeolites

When a ZME whose zeolite contains an electroactive species (ion exchanged in the molecular sieve prior to electrode fabrication) is immersed in an electrolyte solution free of any added electroactive probe, it often displays well-defined electrochemical signals. This is illustrated in Figs. 6–8 for the three electroactive probes the most frequently studied at ZMEs: Ag^+ (Fig. 6), Cu^{2+} (Fig. 7), and methyl viologen MV^{2+} (Fig. 8).

Upon continuous cycling potentials, the height of voltammetric peaks dramatically decreases as a result of progressive depletion of the electroactive probe in zeolite particles located at the electrode surface (e.g., Fig. 6). This is due to ion exchange with cations of the electrolyte solution (24,47,65,67,68,90,104,150). This behavior is opposite to that observed for solution phase electroactive species that concentrate at ZMEs (see Section IV.A.1 and Fig. 5 of this chapter), in agreement with ion-exchange processes in zeolites. The change with time points out that kinetic factors must play a major role since the system is far from equilibrium. A similar decrease in peak intensity was observed by exposing ZME to the electrolyte solution (at open circuit) during a selected time prior to recording the voltammograms (47,48,68), and the phenomenon increased with soaking time (150) and concentration of electrolyte solution (154).

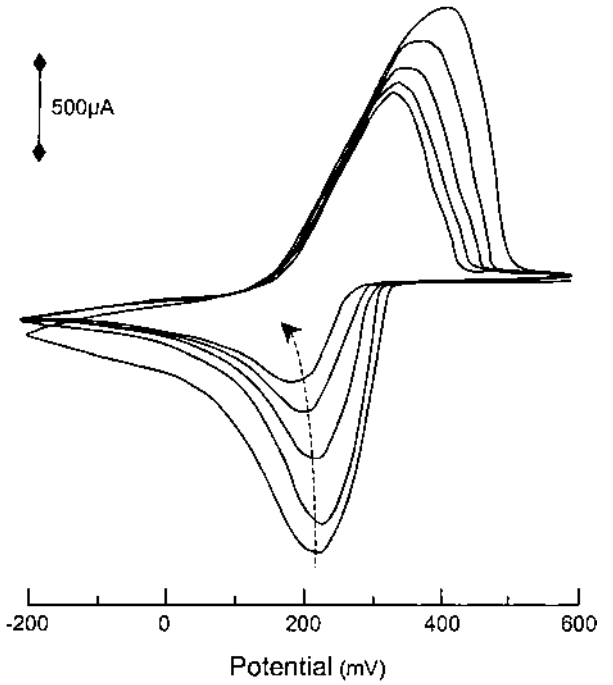

Fig. 6 Cyclic voltammetry of fully exchanged silver zeolite Y, recorded in 0.1 M $LiClO_4$. Scan speed 5 mV/s. The decrease in current for each scan (arrow) is due to ion exchange with the supporting electrolyte ion. (Reprinted with permission from Ref. 104.)

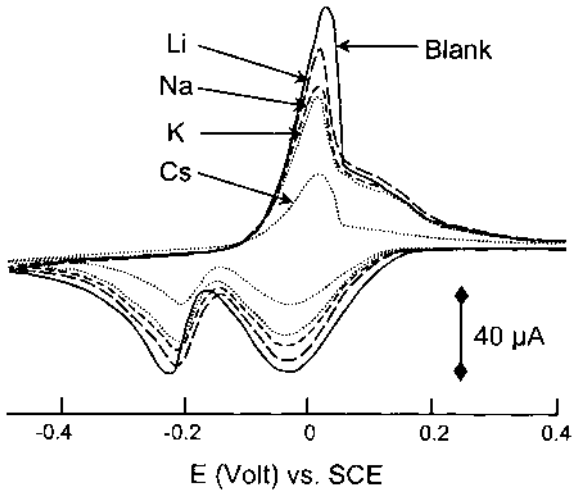

Fig. 7 Cyclic voltammograms of the $Cu_{10.6}Na_{34.8}$-Y-modified electrodes in 0.1 M NaCl aqueous solution after immersion in (Cs) 0.1 M CsCl, (K) 0.1 M KCl, (Na) 0.1 M NaCl, and (Li) 0.1 M LiCl for 20 s. Curve (blank) corresponds to the untreated electrode. The curves were recorded at pH 6, 20°C, a scan rate of 20 mV/s, an initial potential of 0.4 V, and a switching potential of −0.5 V. (Adapted from Ref. 68, with permission.)

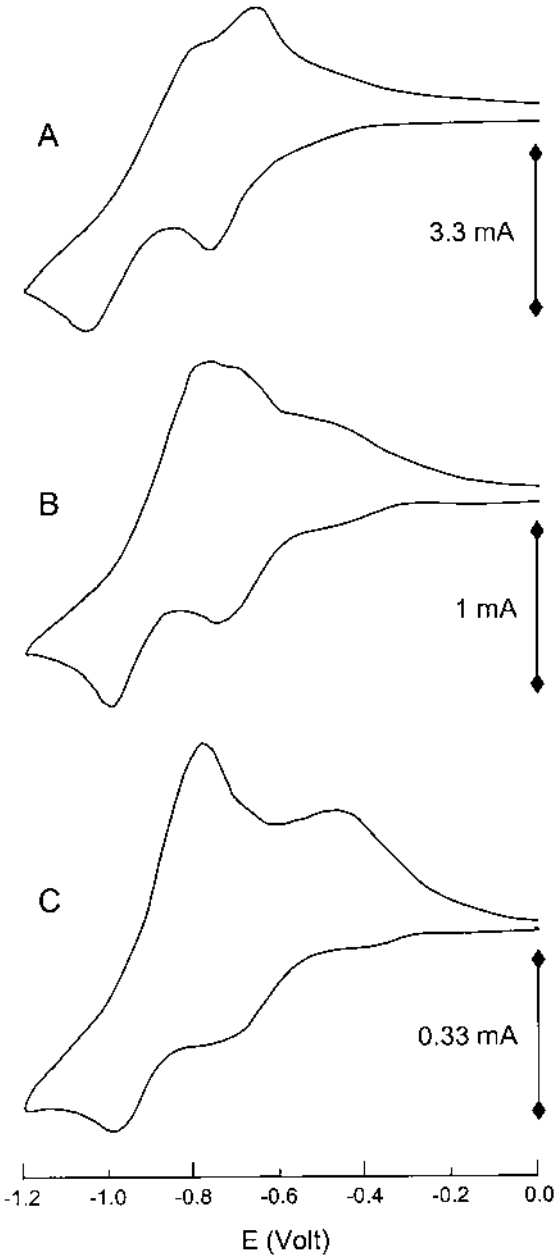

Fig. 8 Cyclic voltammetry of methyl viologen supported on zeolite Y–modified carbon paste electrode in 0.1 M NaCl aqueous solution. Scan rates: (A) 1000 mV/s, (B) 100 mV/s, (C) 10 mV/s. Methyl viologen content in zeolite, 1 mmol/g. (Adapted from Ref. 150, with permission.)

The leaching process is rather fast and depends on the nature of the electrolyte cation (68). For example, experiments carried out immediately after immersion of copper-exchanged ZME in a NaCl electrolyte solution, and after a 20-s treatment in stirred solutions containing either CsCl, KCl, NaCl, or LiCl at the same concentration, show that Cu^{II} species rapidly leach out of zeolites, at a rate in the order $Li^+ < Na^+ < K^+ < Cs^+$ (Fig. 7). This order agrees well with the size of hydrated cations, which govern the speed of the exchange process (in most cages). Accordingly, the electrochemical response of ZMEs exchanged with electroactive species (without any pretreatment) is more intense the smaller the size of the (hydrated) electrolyte cation and the higher its concentration (43,64,68,76,150,167). Peak currents observed for an AgY-modified electrode as a function of quaternary ammonium ion concentration in solution were found to increase linearly with concentration of the non-size-excluded cations, with slopes decreasing in the order $NH_4^+ > NMe_4^+ > NEt_4^+ > NPr_4^+$ (64). The use of the large size–excluded NBu_4^+ species as the electrolyte cation results in nearly insignificant responses attributed to exchange of electroactive probes located on the external surfaces of zeolite particles or slow intrazeolite exchange under forcing conditions (64). Also, the use of ZMEs comprising zeolites of different pore apertures leads to voltammetric peaks that increase in intensity with size of the zeolite pores and channels (for the same particle size) (73,167). All of these observations indicate that diffusion processes play an important role in the overall transformation of an electroactive probe at ZMEs.

This is further proven by the evolution of voltammetric peaks with scan rate (illustrated for MV^{2+} at ZMCPE on Fig. 8). These display a linear dependence of peak height with the square root of scan rate (151), which is typical for diffusion-controlled charge-transfer reactions (188). Such dependency is often observed for ion-exchangeable electroactive species at ZMEs (61,148,159), except when electrochemically distinct ions are involved [several successive signals for the same species, see below (65,70,76,104)], or when leaching the electroactive probe from the zeolite is prevented (57). This latter case has been observed with electrodes coated with zeolite Y containing porphyrin adsorbed onto—and viologen species exchanged inside—the zeolite particles. The porphyrin monolayer effectively seals up the zeolite against exchange of encapsulated viologens with solution phase cations while acting as an electron shuttle between the electrode surface and the viologen entities (57).

One of the most striking points in the electrochemistry of ZMEs is the wide diversity of electrode configurations (especially from the microscopic point of view), which, coupled with the wide range of experimental parameters liable to affect the electrochemical response (all of them being rarely investigated in a single study), makes comparison among the various cases very difficult. Even when applying the same preparation procedure, the resulting ZME will display variable composition and structure at both nano- and microscale levels. This would be very difficult to reproduce exactly, as one can imagine from the oversimplified schematic views of ZMEs depicted on Figs. 1–3. These nano- and microstructures (including those within zeolites), wherein the electroactive guests are liable to experience very different environments, are thought to affect the electrochemical response of ZMEs to various degrees. However, electrochemical measurements provide macroscopic data, often obtained under nonequilibrium conditions, that are related to complex processes occurring in microscopic heterogeneous domains. Although some macroscopic electrochemical data have been successfully exploited to characterize microscopic host–guest effects, i.e., cation site effects or ion-exchange dynamics (66,67,69,70,76,83,104,109,127), this duality of global electrochemical measurement resulting from many different localized nano- and microscopic events remains (in this

author's opinion) the main barrier to the full control and complete understanding of the electrochemical behavior of ZMEs. It is noteworthy that this drawback is largely compensated for by the presence of various attractive applications following fundamental studies (see Section V). In any event, advances in the basic understanding of ZMEs have been achieved, and general trends can be gleaned from analysis of the available literature.

At first glance, it has appears that voltammetric signals obtained with ZMEs that contain exchanged electroactive species, especially those recorded using ZMCPE, do not differ significantly from those resulting from solution phase electroactive probes, at least with respect to their shape and position (47,60,148,150,159). This is in good agreement with the progressive leaching of probes from zeolite particles into the surrounding solution. Nevertheless, electrochemical behavior is clearly affected by type of electroactive probe, ion exchange extent and cation site effects (and therefore zeolite type), electrode composition and configuration, and nature and concentration of supporting electrolyte as well as solvent. Some illustrative examples are now provided.

The first example is the electrochemistry of Ag^+ in zeolite Y. The redox activity of this species is intrinsically simple because "$Ag^+ + 1e^- \rightarrow Ag^{(0)}$" is the only cathodic pathway in the absence of any complexing agent for Ag^+. Indeed, as shown in Fig. 6 for a fully exchanged silver zeolite Y, the voltammetric signals of a film-type ZME is apparently characteristic of only the simple monoelectron reaction $Ag^+/Ag^{(0)}$. However, when decreasing the silver loading in the zeolite, one can distinguish two distinct cathodic peaks (Fig. 9) whose relative ratio is dependent on both temperature and scan rate (104).

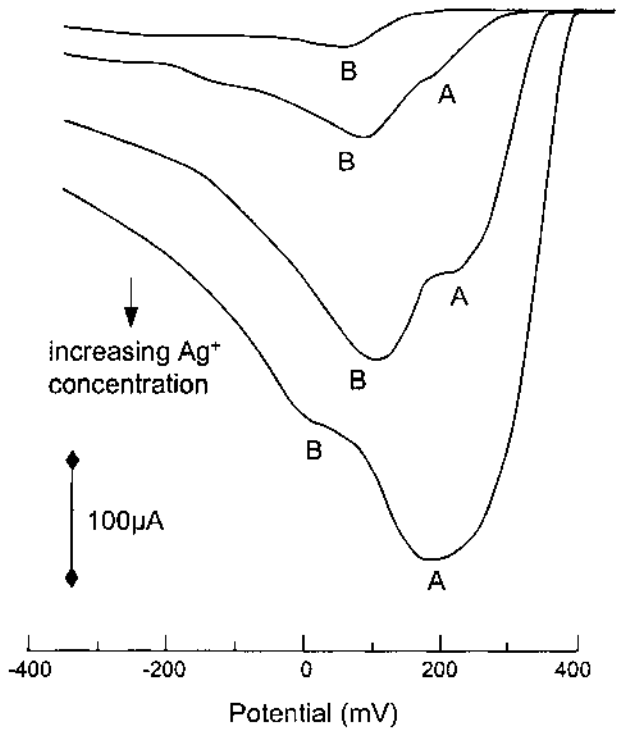

Fig. 9 Cathodic waves observed for silver zeolite Y electrodes as a function of silver ion concentration. Note that as the concentration of silver increases, site B saturates and further silver ion occupancy proceeds through site A. (Adapted from Ref. 104, with permission.)

These two signals (referred to as A and B in Fig. 9) were attributed to Ag^+ ions located in two different ion exchange sites, respectively, on the walls of supercages (site II) and in the hexagonal prisms (site I) (104). Reduction of Ag^+ from site II is easier than that from site I, and occurs at lower cathodic potential values, because site I encompasses Ag^+ in a more confined environment than site II. The relative intensities of peaks A and B are controlled by the Ag^+ ion occupancy in the zeolite. They are governed during the electrochemical experiment by the speed of interconversion of Ag^+ from one site to another, which occurs as a consequence of consumption of either species as a function of the applied potential. The activation energy for intracrystalline ion exchange between the large- and small-channel systems is 35 kJ mol^{-1}, which is significantly higher than that corresponding to counterdiffusion of silver and sodium cations in the large-channel network (30 kJ mol^{-1}), as measured from chronoamperometric experiments (66). This technique is also able to determine the intrazeolite diffusion coefficient, which was reported as 2–4 10^{-8} cm^2 s^{-1} for Ag^+ in zeolite Y (78).

So why does the fully exchanged zeolite not give the two signals? Diffusional processes involving a large amount of Ag^+ in the large channels are so fast that the amount transformed during the electrochemical event is also large and, consequently, leads to large voltammetric peaks that smooth the eventual splitting effect due to various ion-exchange sites. Seeing the less accessible sites requires either low exchange degrees or the use of ZMEs in which the electroactive cations are exclusively located in the more confined sites.

The relative Ag^+ population of sites I and II is also sensitive to the type of cocation. Figure 10A compares the electrochemical response of a zeolite Y containing a small amount of Ag^+ ions distributed randomly in the zeolite structure (sample $Ag_6Na_{50}Y$) with another Y sample containing a little more Ag^+ species but almost exclusively in the small channels ($Ag_{16}Cs_{40}Y$). The voltammetric signals observed with the low-Ag^+ zeolite are much larger. Once again, this behavior is explained by the easy exchange of Ag^+ located in the large cages, whereas those located in the small channels are not accessible to the Cs^+ electrolyte cation (Cs^+ is known to be excluded from the sodalite cages) (64). Even when using an electrolyte cation liable to diffuse into the small cages, very low currents are observed because of the slow interconversion between Ag^+ from small- to large-pore systems (67). This is further exemplified in Fig. 10B for zeolite X. Increasing the Ag^+ content slightly from 3.4 to 5.4 ions per unit cell results in a 50-fold enhancement of the voltammetric response recorded at ZME. This indicates that Ag^+ ions are almost exclusively located in the small-channel network in $Ag_{3.4}Na_{51.8}$-X while some supercage sites are occupied in $Ag_{5.4}Na_{53.5}$-X (83). The electrochemical response of silver species ion exchanged in supercages is governed by the size of hydrated electrolyte cation (as also observed in preconcentration analysis; see Sec. IV.A.1 of this chapter), but the Faradaic currents due to silver initially located in the small cages is monitored by the ionic radii and dehydration energies of the electrolyte cations (67).

On the other hand, no distinct voltammetric peaks have been observed for ZMEs loaded with methyl viologen in zeolite Y (47,71,89,150,154,170), probably because MV^{2+} species are exclusively located in the supercages (189). However, this statement must be qualified because ZMEs made of zeolite A exchanged with silver display complex behavior with several electrochemically distinct species. These species correspond to Ag^+ reduction (70,76), despite the fact that all of the exchange sites are located in the same type of cages (41). The relative intensity of each voltammetric signal is strongly dependent on various experimental parameters (scan rate, supporting electrolyte, Ag^+

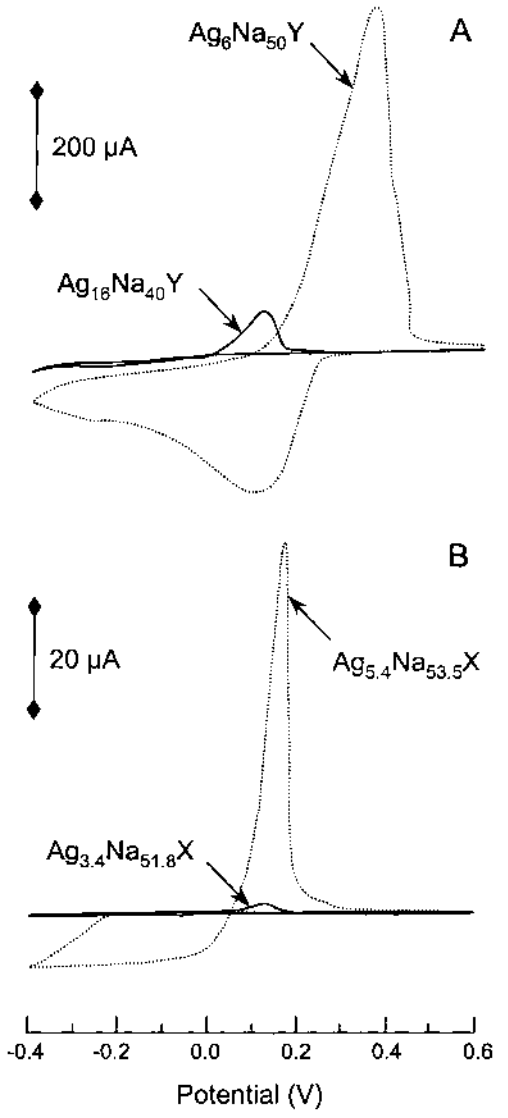

Fig. 10 (A) Cyclic voltammetry of Ag_6Na_{50}-Y- and $Ag_{16}Cs_{40}$-Y-modified electrodes in water containing 0.1 M KNO_3. Reference electrodes were either SCE ($Ag_6Na_{50}Y$) or Pt quasi-reference ($Ag_{16}Cs_{40}Y$). (B) Cyclic voltammograms of $Ag_{3.4}Na_{51.8}$-X and $Ag_{5.4}Na_{53.5}$-X in 0.1 M $NaNO_3$. Scan rate 20 mV/s. (From Refs. 64 (A) and 83 (B), with permission.)

loading, electrode substrate; see Fig. 11), making rigorous interpretation of the data difficult (22,23). To explain the electrochemical data, some authors speculate that the various voltammetric signals are due to different crystallographic Ag^+ sites in zeolite A (70) [with variable coordination strengths (190)], whereas others demonstrate nucleation and growth of metallic silver upon reduction of AgA film-ZME at different sites on the electrode surface (76,191). The latter explanation is supported by chronoamperometric experiments performed at several key potentials (pre and post peaks of the cyclic

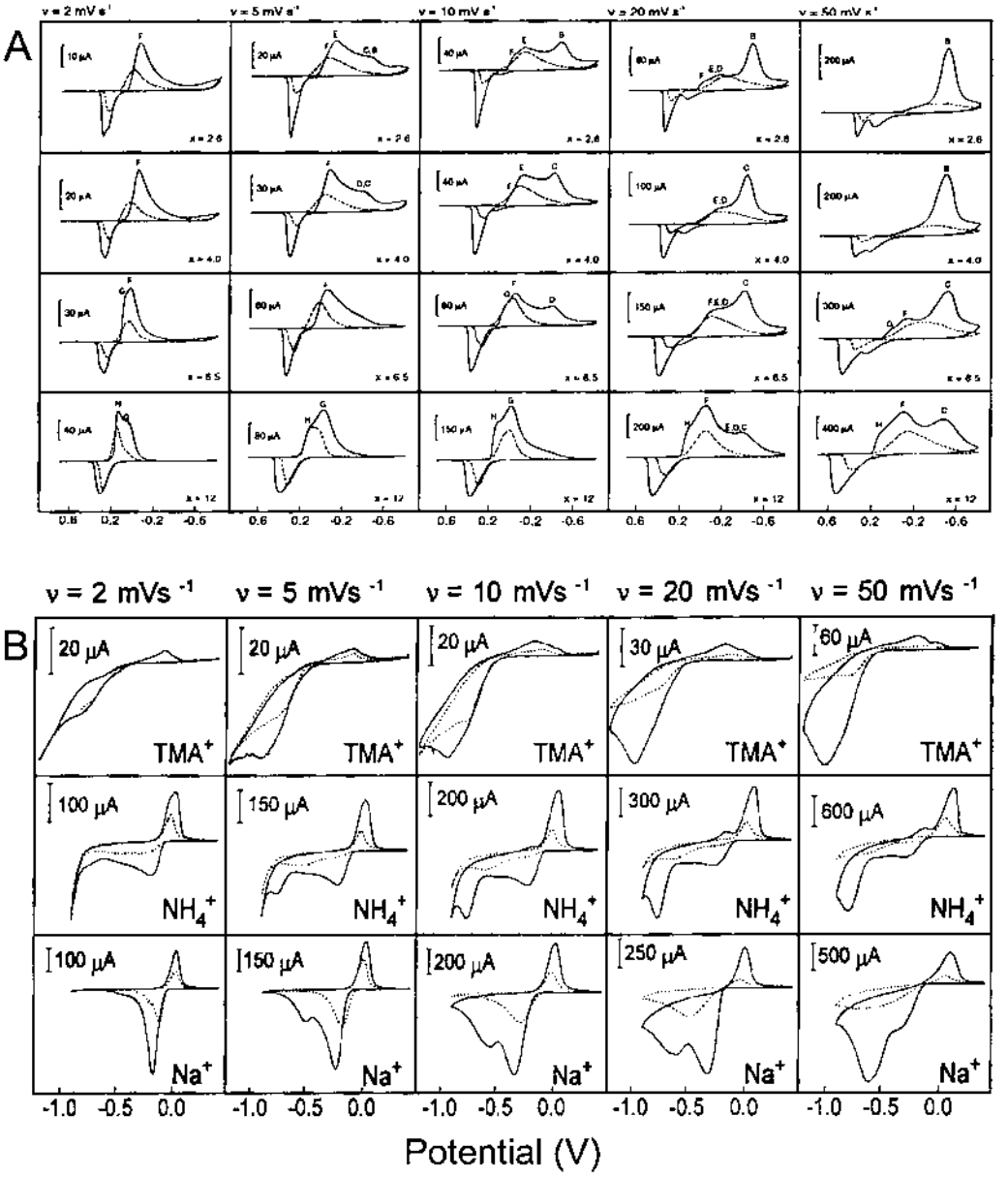

Fig. 11 (A) Voltammetric behavior of Ag^+-A-modified glassy carbon electrodes in 0.1 M $NaClO_4$ as a function of the scan rate and the Ag^+ exchange degree x. Each column corresponds to a different x but the same scan rate, and each row corresponds to a different scan rate but the same x. The solid and dashed lines are the first and the second cycles, respectively. The upper half of traces are the cathodic currents. (B) Effect of electrolyte cation size and scan rate (v) on the cyclic voltammetry of Ag_6A zeolite–modified electrodes in 0.1 M solutions of $NaNO_3$, NH_4NO_3, and $N(CH_3)_4NO_3$. First scan is denoted by a solid line and the second scan by a dashed line. (Reprinted with permission from Refs. 70 (A) and 76 (B). Copyright 1995, 1997 American Chemical Society.)

voltammetric curve), which show growth-and-decay shapes for the current transients (Fig. 12). One may also note in Figure 11 that the amount of Ag^+ reduced during the first forward scan is always much higher than the corresponding anodic stripping peak recorded on scan reversal. This indicates that the totality of metallic silver clusters formed at ZME cannot be reoxidized, some of them having left the electrode surface. This probably occurs via the formation of Ag_x^{n+} (with $n < x$) clusters that are mobile enough to fit inside the zeolite structure and are accommodated in the cages (43,192).

One already knows that supporting electrolyte greatly influences the ZME response via its effects on ion-exchange kinetics (i.e., monitoring mass transport of electroactive species; Fig. 7) and the ability (or not) for its cation to reach specific sites in the zeolite network (Figs. 9 and 10). These characteristics result in peak height variation or growing of additional signals (Fig. 11). Figure 13 shows an additional effect observed with an incompletely exchanged Cu^{2+}-Y zeolite studied at a film ZME in various alkali-metal chloride media, in a potential range where only the Cu^{II}/Cu^{I} redox process occurs. Compared to solution phase copper(II) (adjusted at an appropriate concentration to get cathodic currents nearly equal to those recorded with ZMEs), peak currents and anodic-to-cathodic peak ratios obtained at ZMEs are dependent on the nature of the electrolyte cation M^+. One interpretation is that variation in apparent selectivity coefficients for Cu^{2+}/M^+ and Cu^+/M^+ exchanges, depending on the nature of M^+, results in shifting the apparent formal potential for the Cu^{2+}/Cu^+ couple (68). This shift is observed in addition to variation in peak heights due to the effect of the electrolyte cation on rate-limiting mass transport.

As already suggested above, both composition and configuration of ZMEs can significantly influence the electrochemical response of exchanged electroactive species. An illustrative example is given in Fig. 14 where two experiments were performed on cobalt-exchanged zeolite Y in identical solutions, using the same electrochemical techniques under the same conditions (113,64). The only differences were the electrode type and, probably, the origin of the zeolite sample [only specified in (64)] and the extent of exchange

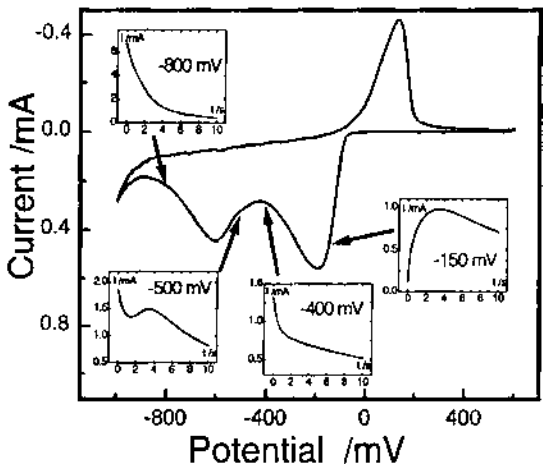

Fig. 12 Cyclic voltammetry of Ag_6A zeolite–modified electrode at a scan rate of 20 mV/s. The insets show chronoamperometry recorded at the indicated potentials. (Reprinted with permission from Ref. 76.)

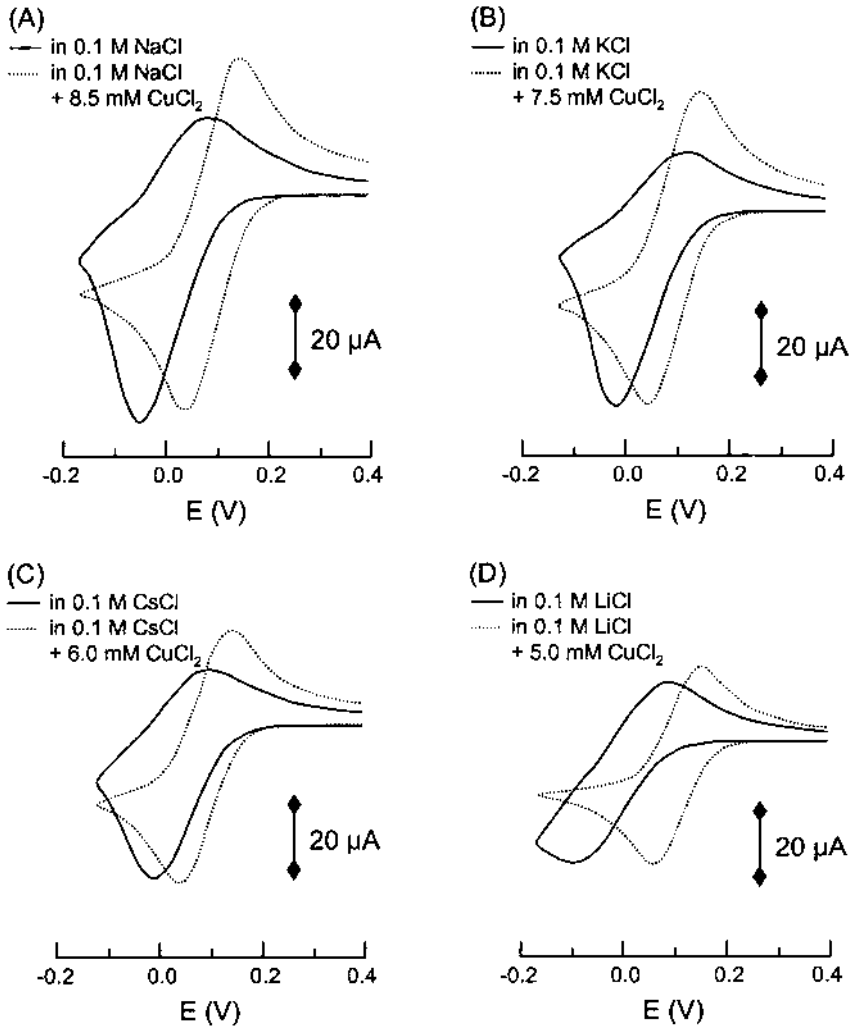

Fig. 13 Cyclic voltammetric behavior of $Cu_{10.6}Na_{34.8}$-Y-modified electrodes (solid curve) and of Cu^{2+} ions at the unmodified glassy carbon electrode (broken curve) in different alkali chloride solutions at 20°C and a scan rate of 20 mV/s. The initial potential is 0.4 V and a switching potentials are (A) −0.17 V, (B) −0.13 V, (C) −0.12 V, and (D) −0.18 V. (Adapted from Ref. 68, with permission.)

[only mentioned in (113)]. In the first case, the electrode was made of pressed zeolite-carbon on a gold grid (113), and in the second a zeolite-carbon-polystyrene film coated on indium-tin oxide was used (64). These systems were investigated in dimethylsulfoxide (DMSO) containing tetrabutylammonium tetrafluoroborate ($TBABF_4$) as the electrolyte to evaluate the electrochemistry of ZME in the presence of size-excluded cation (TBA^+). As clearly shown in Fig. 14, the voltammetric signals are significantly different. Of course, all of them are small because only the cobalt ions exchanged in cages located at the outermost part of the zeolite particles are involved in the electrochemical processes (due to the size-excluded electrolyte cation), but the voltammetric peaks obtained for the pressed

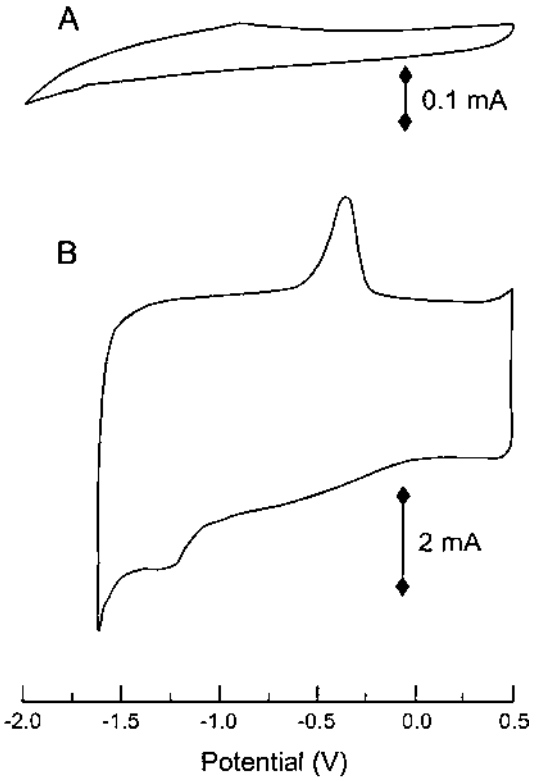

Fig. 14 Cyclic voltammetry of Co^{II}-Y zeolite–modified electrodes recorded in acetonitrile + 0.1 M tetrabutylammonium tetrafluoroborate, at a scan rate of 20 mV/s. (A) Graphite-zeolite-polystyrene film coated on indium-tin oxide electrode; (B) pressed powder composite electrode prepared with graphite and zeolite. (Reprinted with permission from Refs. 64 (A) and 113 (B).)

electrode were higher than with film ZME. This could be interpreted as more efficient carbon-zeolite contact in the first case (suggested by the large effective electrode surface area, owing to large capacitive currents), whereas polystyrene can hinder the contact between zeolite and the current collector in the second case. But the lack of comparison data (i.e., Co^{2+} loading and relative location in the exchanging sites) limits somewhat the drawing of adequate conclusions. This example illustrates the importance of the preparation step and resulting design of ZMEs on response, as well as the need for reporting a full characterization of the zeolite materials used to build ZME, including a detailed presentation of any modifications.

Finally, solvent has been found to affect the voltammetric behavior of ZMEs. First, solvent can act on the ion-exchange reactions in zeolites (on both equilibrium and kinetics) that are controlling the electroactivity of species in ZMEs. As an example, the voltammetric cathodic peak of AgA in pure dimethylformamide (DMF) is 500 times smaller than in water (63). Adding progressively increasing amounts of water to DMF results in proportional peak height growth due to the rate-accelerating action of water on the ion exchange process, leading to more detectable silver (63,193). Second, solubility effects can arise as a consequence of the electrochemical transformation. This is the case for methyl viologen, which undergoes two successive electron transfers in the cathodic

direction, $MV^{2+} \rightarrow MV^{\bullet+} \rightarrow MV^{(0)}$, where MV^{2+} and $MV^{\bullet+}$ are hydrophilic while $MV^{(0)}$ is hydrophobic. This in turn leads to significant differences in the voltammetric curves recorded in either aqueous or nonaqueous media (47). Third, solvation effects might be affected by zeolite type. This is illustrated in Fig. 15, where responses of CuY- and CuA-ZMEs are compared in DMSO solutions containing increasing water contents (24). Both Cu^{2+} and Cu^{+} form solvated complexes with DMSO. While CuY-ZME displays significant voltammetric signals due to fast ion exchange between solvated Cu^{II} and electrolyte cation, the electroactivity of Cu^{II} in zeolite A is prevented in pure DMSO because this solvent molecule cannot enter the small zeolite A structure. Addition of water is necessary to recover voltammetric signals for CuA-ZME, which allows charge compensation to proceed by exchanging Cu^{2+} for electrolyte cation (Fig. 15).

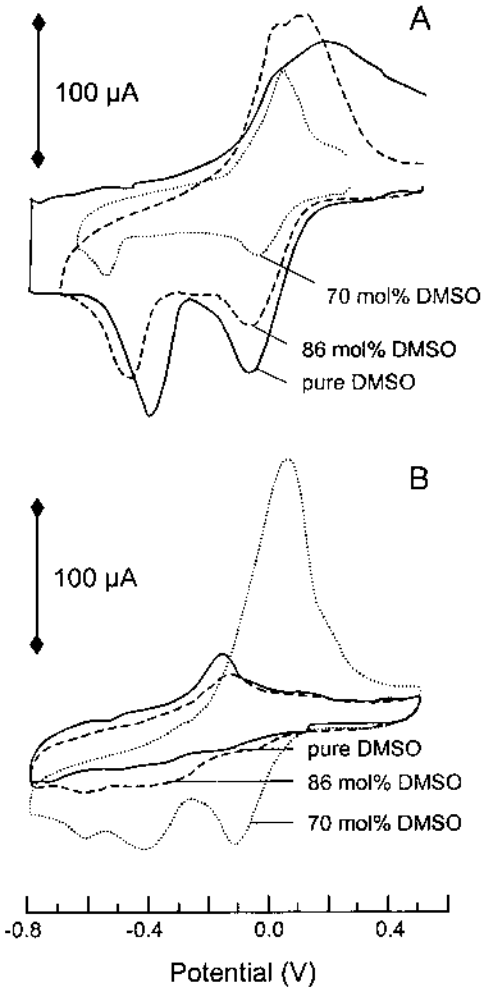

Fig. 15 Cyclic voltammograms recorded as a function of the composition of the solvent. Electrolyte was 0.1 M KNO_3 in all cases and scan rate equal to 10 mV/s: (A) CuY; (B) CuA. (Reprinted with permission from Ref. 24.)

3. Electrochemical Activity of Electroactive Species Physically Entrapped in Zeolites

If a ZME contains electroactive species that have been encapsulated as ship-in-a-bottle complexes in the porous zeolite network, its electrochemical behavior is fundamentally different from those containing ion-exchanged electroactive probes. This arises from the very limited degree of freedom (restricted movement inside the rigid structure) experienced by these physically entrapped moieties. Nevertheless, electroactive complexes encapsulated in ZMEs give rise to electrochemical signals (see examples below), but their real origin has been controversial (9,11,22–26,109,194). The electrochemistry of zeolite-encapsulated complexes has been largely studied by Bedioui's group (18,20,112–119,121–123,127), as well as some others (24,79,87,108,109,185).

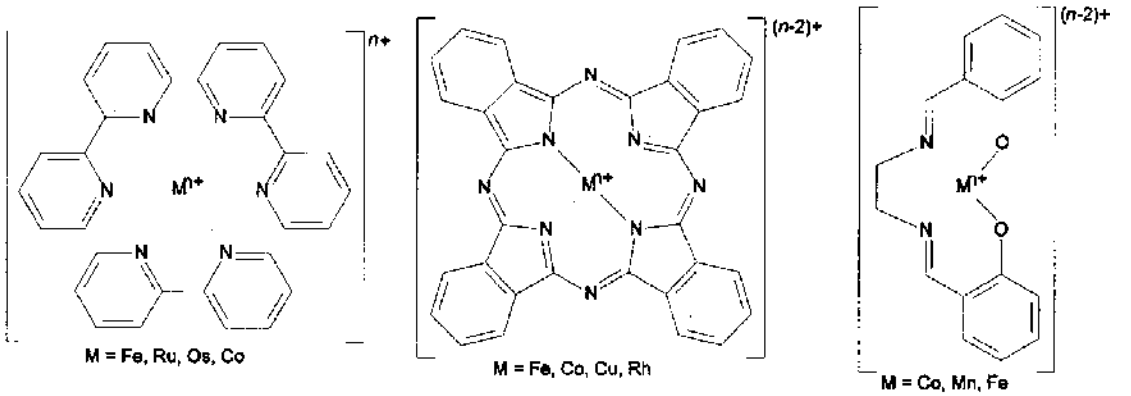

Metal *tris*-bipyridine | Metal phthalocyanine | Metal-salen

In addition to large species simply adsorbed onto the external surface of zeolite particles, such as porphyrins (45,57,120), the size-excluded electroactive probes that have been studied in electrochemistry as encapsulated complexes are of three types: metal–tris-bipyridine moieties, metal-phthalocyanines, and metal–Schiff base complexes (see above). These are most often synthesized directly inside the molecular sieve by allowing a metal-exchanged zeolite to react with the appropriate ligand, but synthetic procedures involving the zeolite building around the preformed complexes have also been reported (112,122). On the basis of their state of confinement, one can distinguish three kinds of environments experienced by the complexes: (a) the outermost external surface where complexes are simply bound to the particle surface (adsorbed or ion exchanged) and can be readily displaced in solution under appropriate conditions; (b) the first layer of complete or broken cages located at the particle boundary where complexes are (at least partially) occluded in or in strong interaction with these cages, so that they cannot easily leave their site but can be readily reached by the external solution; and (c) the bulk zeolite where complexes are entirely entrapped in the three-dimensional lattice and therefore cannot move from one site to another and of course cannot leave the zeolite structure (unless being decomposed, i.e., by removal of ligands). The first two environments are likely to participate in an electrochemical reaction due to their direct contact with a conducting substrate (i.e., electrode feeder), close enough to allow the electron transfer. However, the redox transformation of complexes located

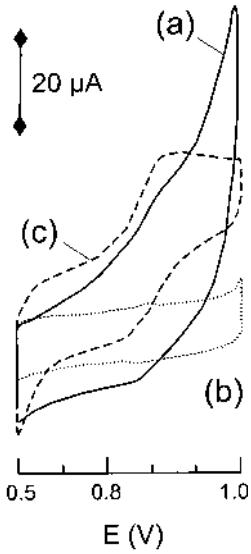

Fig. 16 Cyclic voltamograms of $[Fe(bpy)_3]^{2+}$-Y-coated electrodes dipped in 0.1 M Na_2SO_4 (a), after continuous cycling for 1 h (b), and after addition of 0.05 M H_2SO_4 (c) (scan rate = 50 mV/s, $[Fe(bpy)_3]^{2+}$-Y = 43 μmol/g. Fe(II) complex present in the cage = 28 μmol/g. Fe(II) complex adsorbed on the surface = 15 μmol/g. (Reprinted with permission from Ref. 79.)

deeper in the bulk zeolite (if occurring)* would require either a mobile non-size-excluded mediator or very close contact of encapsulated species to facilitate electron hopping between them [as was demonstrated for photoassisted electron transfer in the channel molecular sieve structure of zeolite L (189)].

Following are some examples and conclusions regarding the electrochemistry of ZMEs containing the three electroactive species represented in Scheme 1. $Fe(bpy)_3^{2+}$ encapsulated in zeolite Y displays voltammetric behavior at ZME similar to that in solution with, however, a slight shift in peak potentials (114). Peak heights, relative to either the oxidation of Fe^{II} or bipyridyl-centered reduction, are rather low because only a small fraction of the entrapped species is effectively electroactive. Grinding the zeolite particles prior to electrode modification, leading to a higher surface-to-volume ratio, can enhance signals (194). On the other hand, lengthening the mechanical working of zeolite-graphite composites (by increasing the pressure time) results in a significant decrease in peak current, which is nearly complete for Fe^{II}-centered oxidation (109). When using a film-based ZME made of zeolite Y containing a low loading of $Fe(bpy)_3^{2+}$ species (1 per 17 supercages), the electrochemical response recorded in a sodium sulfate solution is small and tends to disappear after 1 h of continuously cycling potentials (Fig. 16). This is due to progressive leaching of the surface-bound complexes (that are mainly at the origin of peak currents) into the external solution, while the remaining $Fe(bpy)_3^{2+}$ in the first layer of complete or broken

* To date, no deep bulk intrazeolite electrochemical transformation of encapsulated complexes has been reported because less than 2% (between 0 and 2%, depending on the cases) of the entrapped species were found to be electrochemically active, which corresponds essentially to both surface or boundary cages layer sites.

cages located at the particle boundary are not sufficiently numerous to provide a significant electrochemical response [which requires higher concentrations (127)]. To reveal the electrochemical activity of bulk $Fe(bpy)_3^{2+}$ species, it is necessary to work in the presence of strong acid (Fig. 16) that disintegrates the zeolite structure with concomitant leaching of the bulk complexes into solution in close proximity to the electrode surface (79). Similar results are obtained for the zeolite Y-$Ru(bpy)_3^{2+}$ system (79). On the other hand, pressed zeolite-carbon-based ZMEs made of zeolite Y containing a high loading of either $Ru(bpy)_3^{2+}$ or $Co(bpy)_3^{2+}$ species (nearly one per supercage) reveal more intense voltammetric signals persisting (and giving rise to peak splitting) after long exposure of the electrode to the solution (4 days), even after transfer to a new electrolyte solution [see Fig. 17 for $Co(bpy)_3^{2+}$]. Both the peak splitting behavior and the unfavorable comparison to pure solid or solution phase $Co(bpy)_3^{2+}$ indicate that interaction with the zeolite structure affects the ZME response (127). When studied over a wider potential range, additional signals are also observed for the zeolite Y-$Ru(bpy)_3^{2+}$ system and were attributed to species entrapped in more confined near-surface sites (11,127).

Co^{II} and Fe^{II} phthalocyanines as well as Co^{II} and Cu^{II} hexadecafluorophthalocyanines were investigated voltammetrically as encapsulated complexes in zeolites X and Y

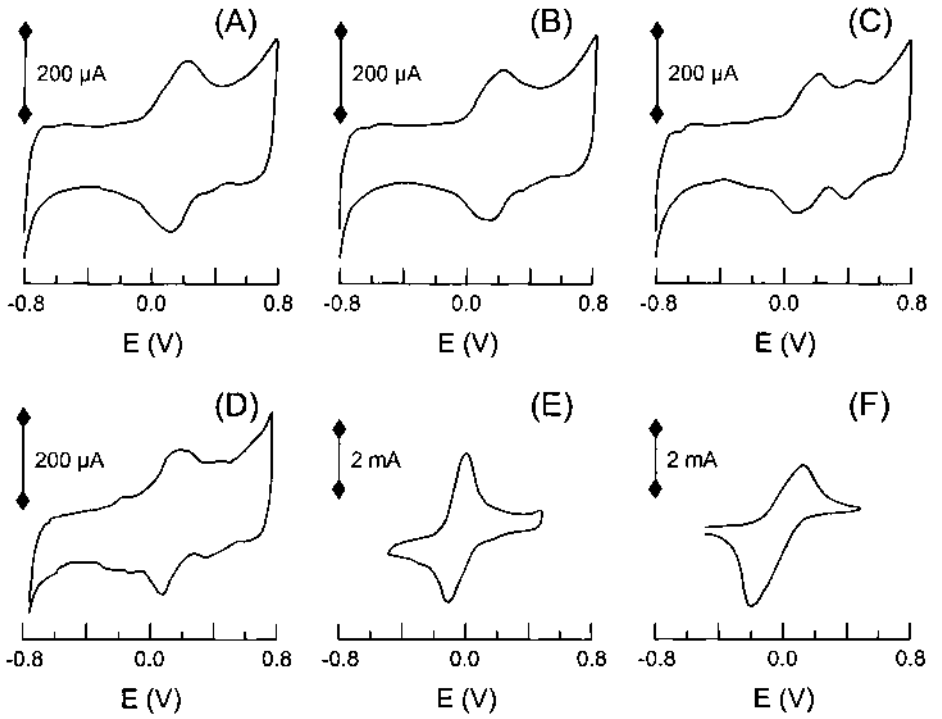

Fig. 17 Cyclic voltammograms of $[Co(bpy)_3]^{2+}$-Y at a pressed powder graphite electrode in 0.1 M KNO_3 aqueous solution few minutes (curve A), 6 h (curve B), and 96 h (curve C) after the immersion of the electrode into the solution; and after transfer of the electrode to a new electrolyte solution (curve D); potential scan rate was 20 mV/s. Curves E and F were respectively obtained in 0.1 M KNO_3 solution containing 1.7 mM dissolved $[Co(bpy)_3]^{2+}$, with using a pressed powder composite electrode prepared with 25 mg graphite and 25 mg zeolite NaY (curve E), and in 0.1 M KNO_3 solution at a pressed powder composite electrode prepared with 25 mg graphite, 25 mg zeolite NaY, and 10 mg $[Co(bpy)_3]^{2+}$ (curve F). (Adapted from Ref. 127 with permission.)

(108,112,116–118,122). In general, their behavior is similar to that observed for monomers in solution, but they usually display better defined signals due to confinement that prevents the aggregation of complexes, which is known to induce kinetic complications in solution (122). Also, site isolation of Rh^{III} phthalocyanine in zeolite Y enables the observation of reversible behavior for this complex at ZME (only species trapped in the outermost supercages are electroactive (123) while giving irreversible voltammetric peaks when studied as solution phase species because of dimerization upon reduction Rh^{III}/Rh^{II} (195).

Because of their catalytic properties, redox-active transition metal-salen complexes [where salen = *N*,*N*′-bis(salicylidene)ethylenediamine] have been widely investigated as encapsulated solutes in zeolites at ZMEs (24,87,109,113,115–117,119,121,124). As shown in Fig. 18, the electrochemical behavior of Co(salen)-Y can be different from that in

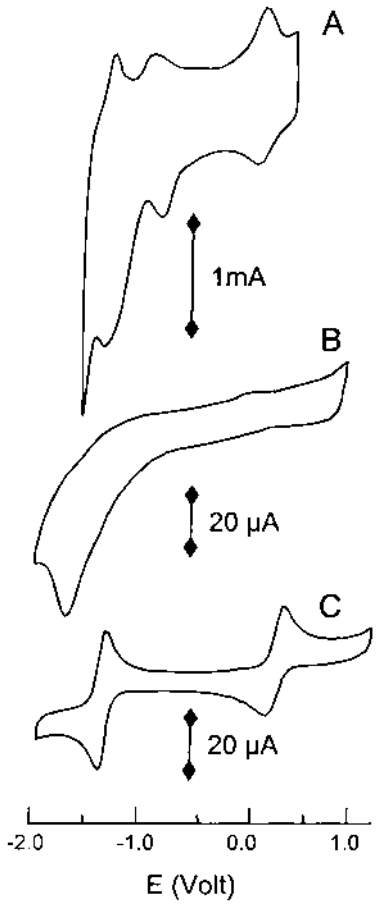

Fig. 18 Cyclic voltammograms of Co(salen) in acetonitrile. (A) Recorded in 0.1 M tetrabutylammonium tetrafluoroborate, at a scan rate of 10 mV/s, with using a pressed powder composite electrode prepared with graphite and zeolite Co(salen)-NaY; (B) recorded in 0.1 M $LiClO_4$, at a scan rate of 50 mV/s, with using a film zeolite–modified electrode made of graphite + zeolite Co(salen)-NaY coated on glassy carbon and covered with an acrylic-based polymer; (C) recorded in homogeneous Co(salen) solution + 0.1 M $LiClO_4$, at a scan rate of 50 mV/s, with using an unmodified glassy carbon electrode. (From Refs. 113 (A) and 24 (B and C).)

solution and is significantly dependent on environmental differences experienced by the species in the confined spaces in ZME. While distinct peaks for the Co^{III}/Co^{II} redox couple and reversible Co^{II}/Co^{I} process were observed by cyclic voltammetry at a pressed zeolite-carbon electrode (113), similar curves recorded using a zeolite-carbon-polymer film exhibited lower signals for the Co^{III}/Co^{II} redox system and a less reversible signal for Co^{II}/Co^{I} transformation, at potential values close to those in solution (24). Variations in the voltammetric signals were also obtained when using various forms of carbon to prepare the electrode (24). Yet another example of different behavior was observed for Co(salen)-Y from dispersion cyclic voltammetry [from Co(salen)-Y zeolite particles suspended in solution between two feeder electrodes], displaying two quasi-reversible Co^{III}/Co^{II} and Co^{II}/Co^{I} couples similar to solution phase species (Fig. 19). Also, a Co(salen)-Y zeolite sample subjected to a high-pressure mechanical treatment prior to voltammetric evaluation resulted in significantly different behavior (Fig. 19). It is noteworthy that synthesis and purification procedures used to get Figs. 18 and 19 could have led to various compositions of the Co(salen)-Y zeolite (24,109,113). These aforementioned studies highlight several parameters that influence the electrochemical of Co(salen)-Y-based ZMEs, such as the encapsulation method, the ratio between surface and bulk encapsulated complexes, their coordination in the solid, the mechanical working of zeolites, and the electrode composition and configuration. Additional data are available for zeolite-encapsulated $Mn(salen)^{+}$ and $Fe(salen)^{+}$ (87,115,117,119,121), $Ru(salen)^{+}$ (116), and V(O)salen (124). For example, $Fe(salen)^{+}$-Y displays an electrochemical behavior that is primarily due to the reduction of Fe^{III} centers of complexes either simply bound to the

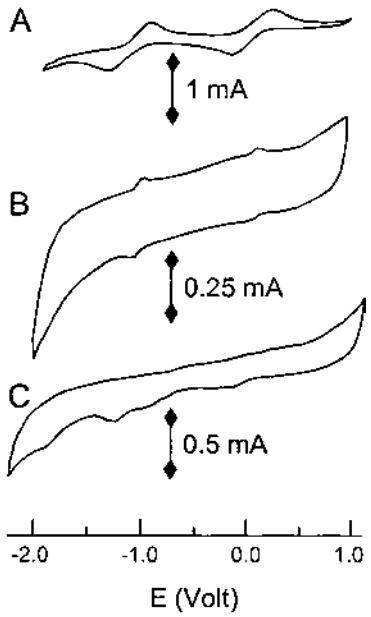

Fig. 19 Dispersion cyclic voltammetry. Cyclic voltammetry in $LiClO_4$/DMF at large area reticulated vitreous carbon electrodes; scan rate = 50 mV/s. (A) 1 mM Co(salen) in homogeneous solution, in 0.2 M $LiClO_4$; (B) dispersion of CH_2Cl_2-extracted, air-exposed Co(salen)-NaY, in 0.2 M $LiClO_4$; (C) dispersion of CH_2Cl_2-extracted, air-exposed Co(salen)-NaY after pressing for 30 min at 14 000 lb/in.^{2} (gauge), in 0.1 M $LiClO_4$. (Adapted from Ref. 109, with permission.)

zeolite surface or occluded in the first layer of complete or broken cages located at the particle boundary (Fig. 20, curve a). When using $Fe(salen)^{+}$-Y particles for which the surface has been covered by adsorbed $Co(dmbpy)_3^{2+}$ species (dmbpy = 4,4′-dimethyl-2,2′-bipyridine), the resulting voltammogram (Fig. 20, curve b) shows a response similar to the direct Fe^{III}/Fe^{II} process, concomitant with the existence of a significant cathodic peak due to the electrocatalytic reduction of bulk $Fe(salen)^{+}$ species by electrogenerated $Co(dmbpy)_3^{+}$ (117). Indeed, the peak current recorded for the Co^{II}/Co^{I} process was much higher than that for surface-adsorbed $Co(dmbpy)_3^{2+}$-Y zeolite particles without $Fe(salen)^{+}$ (comparison between curves b and c in Fig. 20). This example illustrates the mediation power of surface-adsorbed electrocatalysts to induce charge transfer to encapsulated complexes, as otherwise demonstrated for ion-exchanged species in spatially structured systems (56,57,178). However, comparison between the $Fe(salen)^{+}$ response obtained with and without the electron transfer mediator [adsorbed $Co(dmbpy)_3^{2+}$] suggests that only a very limited fraction of complexes encapsulated in the bulk zeolite are attainable this way, most of them remaining electrochemically silent. Using zeolites containing both $Fe(salen)^{+}$ and Ag^{+} allows for a similar increase in the electrochemical accessibility of zeolite-encapsulated complexes, which is then enhanced by electrogenerated silver particles (119).

Because electrochemistry at ZME containing encapsulated complexes only experiences the species present in the outermost layers of the zeolite grains, it is combined with bulk analytical techniques to assess the different nature and distribution of the entrapped compounds. This has been exemplified with Mn(salen) complexes (87). The ship-in-a-bottle

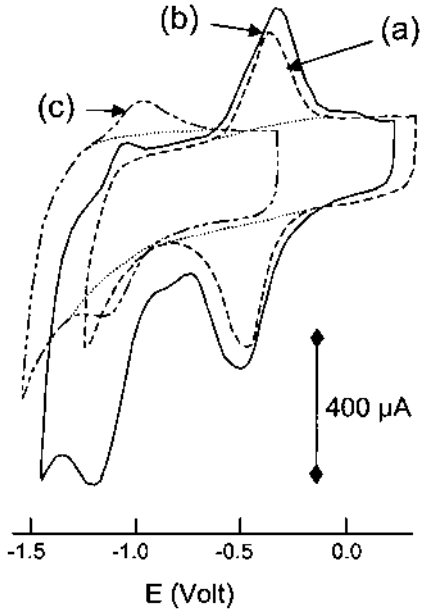

Fig. 20 Cyclic voltammograms of a pressed graphite powder composite electrode containing Y zeolite, recorded in DMSO + 0.1 M $LiClO_4$ (potential sweep rate, 10 mV/s). (a) Y zeolite–encapsulated $[Fe^{III}(salen)]^{+}$ alone; (b) Y zeolite surface–adsorbed $[Co(dmbpy)_3]^{2+}$ and bulk-encapsulated $[Fe^{III}(salen)]^{+}$; and (c) Y zeolite surface–adsorbed $[Co(dmbpy)_3]^{2+}$ alone. (Adapted from Ref. 117, with permission.)

synthesis of $Mn(salen)^+$ within microporous solids requires multistep formation from Mn^{II} salts, which are oxidized to Mn^{III} by molecular oxygen. The oxidation step is usually incomplete in the bulk zeolite (typically 15–20%), as evidenced by EPR spectroscopy. In contrast, electrochemical measurements have revealed a predominance of Mn^{III} at the external surface, indicating that oxidation is only complete in the outermost layers of zeolite particles (87). The presence of Mn^{V} in these regions was also detected by electrochemistry (while not observable by spectroscopy), highlighting the importance of electrochemistry at ZME as a surface characterization tool capable of refining data obtained with bulk analytical techniques.

4. Electrochemistry of the Molecular Sieve Alone

Electrochemical experiments carried out with the zeolite alone have existed for a long time (37–39); voltammetric curves are obtained from pressed pellets heated to 200–500°C, where zeolite becomes ionically conductive. Strictly speaking, the electroactivity is due to the charge-compensating countercations present (i.e., Na^+ or Cd^{2+} in zeolite A), and not to any real transformation of the zeolite network or one of its components. Similar electroactivity of heated dry zeolite crystals doped with various metal species was also reported (129,130). The first study dealing with the electrochemical transformation of the zeolite backbone is a cyclic voltammetric investigation of a mordenite gel in poly(ethylene oxide) oligomers (196). It shows destruction of the Al-O bond at an anodic potential close to 1 V and the extrusion of $Al(OH)_3$ on scan reversal.

Less destructive approaches with ZMEs have been applied to characterize the electrochemical behavior of molecular sieves containing elements isoelectronic with Al^{3+} or Si^{4+} substituted into the framework lattice. The voltammetric behavior of titanosilicalite reveals the possible reduction of tetrahedrally coordinated Ti^{4+} to Ti^{3+}, without apparent expulsion of titanium from the framework sites (149). The electron transfer reaction, which gives quasi-reversible signals in cyclic voltammetry [similar to $Ti(OC_2H_5)_4$], implies diffusion of electrolyte cations to these sites for ensuring charge compensation. Due to the insulating character of the material, the redox process is very likely restricted to the sites located at the outermost surface. Titanosilicalites with various Si/Ti ratios gave peak heights directly proportional to the Ti amount up to 2 wt % Ti content (153). On the other hand, three peak couples characterize the voltammetric behavior of Ti-beta zeolites: one originates from Ti leached in solution and the other signals are related to two framework Ti populations (88). It has been suggested that these could be due to Ti tetrahedrally coordinated to the framework, and the other, which is sensitive to the coordinating ability of electrolyte counteranions, would correspond to surface titanol groups.

Vanadium silicalites and vanadium aluminophosphates can be electrochemically reduced via their V^{5+} centers. Cyclic voltammetry at corresponding ZMEs usually displays two distinct signals, which are both attributed to the V^{5+}/V^{4+} couple resulting from structurally distinct sites (20,107,125,126). In spite of these confinement effects, the electrochemical response is mainly due to the boundaries of the molecular sieve particles as sustained by the rather low accessibility of the redox active sites (only a few percentage points) (126).

In cyclic voltammetric studies of electrically conducting octahedral molecular sieves such as natural and synthetic synthetic heulandite and todorokite, either as such or ion-exchanged with copper(II) species, framework manganese and tunnel copper cations were distinguished (197). Impedance spectroscopy was also applied to zeolite single crystals to characterize their conductivity under various conditions (198).

B. Interplay Between Charge Transfer and Mass Transport: Electron Transfer Mechanisms

The numerous examples depicted in Figs. 5–20 illustrate the rich electrochemical activity of ZMEs. They also point out that multiple experimental factors are affecting the electron transfer processes and that mass transport plays a very important role in the overall redox transformation. A central and intrinsically basic question regards the way in which the electrons are transferred to (or from) an electroactive species located in the rigid microporous structure of an insulating zeolite material. This has generated substantial research efforts and several controversial discussions in the ZME literature. These will not be elaborated upon here, but the interested reader is directed to critical reviews (9,11), comparative works (20,24,109,127), and comments (22,23,25,26).

The two main requirements for an electroactive probe ion exchanged or encapsulated in a zeolite network to undergo a charge transfer reaction are the following:

1. The electroactive species must be connected to a conductive electrode material (either in physical contact to the electrode, close enough to experience direct electron transfer, or mobile enough to freely diffuse to the electrode surface); alternatively, the electroactive species can undergo indirect charge transfer by way of either a suitable mediator that can act as a relay between the electrode and the probe (electrocatalysis) or a sufficiently high density population of the electroactive probes that allows self-exchange of electrons between them (electron hopping);
2. Charge balance must be maintained in the zeolite; therefore, the overall charge-transfer reaction is inevitably associated with a mass transport process: at any time the amount of fixed negative charges in the zeolite network must be counterbalanced by an equivalent amount of cation, so that any reduction of a cationic probe initially exchanged in the zeolite would require the ingress of another cationic species in the bulk material; similar charge compensation would be achieved by cation expulsion from the zeolite upon oxidation of the electroactive probe.

This interplay between charge transfer and mass transport is at the origin of the mechanisms proposed in the literature to explain the electrochemical behavior of ZMEs, and underscores the key role played by diffusion of both electroactive probes and electrolyte cations in affecting the voltammetric responses.

According to the original model of Shaw and coworkers (48) and subsequent amendment by Dutta and Ledney (19), three distinct pathways for describing charge-transfer reactions occurring at ZMEs can be operative. Beside the purely intrazeolitic [Eq. (1)] or extrazeolitic [Eqs. (2a) and (2b)] electron transfer processes, the concept of surface-mediated charge transfer [Eqs. (3)–(5)] was introduced by distinguishing between bulk- and surface-located ion-exchange sites.

Mechanism I:

$$E^{\mathrm{m}+}_{(Z)} + \mathrm{n}e^- + \mathrm{n}C^+_{(S)} \Leftrightarrow E^{(\mathrm{m}-\mathrm{n})+}_{(Z)} + \mathrm{n}C^+_{(Z)} \tag{1}$$

Mechanism II:

$$E^{\mathrm{m}+}_{(Z)} + \mathrm{m}C^+_{(S)} \Leftrightarrow E^{\mathrm{m}+}_{(S)} + \mathrm{m}C^+_{(Z)} \tag{2a}$$

$$E^{\mathrm{m}+}_{(S)} + \mathrm{n}e^- \Leftrightarrow E^{(\mathrm{m}-\mathrm{n})+}_{(S)} \tag{2b}$$

Mechanism III (three subgroups):

$$E^{m+}_{(Z,surf)} + ne^- + nC^+_{(S)} \Leftrightarrow E^{(m-n)+}_{(Z,surf)} + nC^+_{(Z,surf)} \quad (3a)$$

$$E^{(m-n)+}_{(Z,surf)} + nC^+_{(Z,surf)} + E^{m+}_{(Z,bulk)} \Leftrightarrow E^{(m-n)+}_{(Z,bulk)} + nC^+_{(Z,bulk)} + E^{m+}_{(Z,surf)} \quad (3b)$$

$$M^{m+}_{(S)} + ne^- \Leftrightarrow M^{(m-n)+}_{(S)} \quad (4a)$$

$$M^{(m-n)+}_{(S)} + nC^+_{(S)} + E^{m+}_{(Z,surf)} \Leftrightarrow E^{(m-n)+}_{(Z,surf)} + nC^+_{(Z,surf)} + M^{m+}_{(S)} \quad (4b)$$

$$M^{m+}_{(Z,surf)} + ne^- + nC^+_{(S)} \Leftrightarrow M^{(m-n)+}_{(Z,surf)} + nC^+_{(Z,surf)} \quad (5a)$$

$$M^{(m-n)+}_{(Z,surf)} + nC^+_{(Z,surf)} + E^{m+}_{(Z,bulk)} \Leftrightarrow E^{(m-n)+}_{(Z,bulk)} + nC^+_{(Z,bulk)} + M^{m+}_{(Z,surf)} \quad (5b)$$

where E is the electroactive species with charge m+, C^+ represents the electrolyte cation (chosen as monovalent for convenience), M is a mediator (chosen with charge m+ for convenience), the subscripts z and s refer to the zeolite phase and the solution, respectively, and the subscripts surf and bulk refer to the zeolite surface (either external surface or outermost subsurface layer of cages) and bulk ion-exchange sites.

Mechanism I is purely intrazeolitic, where the electroactive species undergoes intracrystalline electron transfer while charge balance is maintained by solution phase electrolyte cations entering the zeolite framework [Eq. (1)]. Note that this mechanism does not distinguish between species located deep in the bulk zeolite and those situated in the boundary region of the zeolite grains. Mechanism II is purely extrazeolitic and involves the ion exchange of the electroactive probes for the electrolyte cations [Eq. (2a)] prior to their electrochemical transformation in the solution phase [Eq. (2b)]. The group of mechanisms III distinguishes between the electroactive probes located in the bulk zeolite and those situated at the external boundary of the particle. The first case is the direct electron transfer to electroactive species situated at the outer surface of the zeolite particles (i.e., those easily accessible to the electrons), with charge compensation ensured by the electrolyte cation [Eq. (3a)]. This step can be (but is not necessarily) followed by electron hopping to the probes located in the bulk of the solid, with concomitant migration of the electrolyte cation inside the zeolite structure [Eq. (3b)]. In the presence of a charge-transfer mediator either dissolved in solution or adsorbed on the zeolite surface, electrochemical transformation [Eqs. (4a) and (5a)] can lead to indirect charge transfer to either surface-confined or bulk-located electroactive probes [Eqs. (4b) and (5b)]. Although some unambiguous evidence is available to support one or another of these mechanisms, all of these theoretical pathways have yet to be demonstrated at practical levels.

More versatility can be added to these mechanistic pathways by defining topological regions of a zeolite as experienced by an electrochemical probe molecule. This concept was introduced by Bessel and Rolison (109), according to a terminology that was previously specified for photoelectron transfer reactions in zeolites (199). Four topological redox isomers can be designated: (a) the solution phase redox solute originating from the zeolite interior; (b) the electroactive probes located at the zeolite boundary (either adsorbed on

the outer surface or occluded in defect sites, or even encapsulated in the outermost layer of the zeolite particle); (c) the redox probes situated in the bulk zeolite but free to experience the global pore lattice over the time scale of the experiment; and (d) the electroactive solutes strictly confined in the zeolite interior by physical entrapment preventing them from motion from one site to another. In the various mechanisms described by Eqs. (1)–(5), the first species are assigned as "S" (solution phase), the second as "surf" (zeolite surface boundary), and the third and fourth as "bulk" (zeolite interior).

Based on the electrochemical behaviors described above (see Sec. IV.A of this chapter), and others from the literature, a briefly summarized (and consequently restricted) view of the actual situation dealing with electron transfer mechanisms at ZMEs, is the distinction between two categories of solutes in zeolite:

1. Ion-exchangeable electroactive probes that are mobile in the zeolite lattice and can therefore be subjected to ion exchange with the electrolyte cations. These undergo extracrystalline electron transfer according to mechanism II [Eqs. (2a) and (2b)]. Several experiments indicate that a chemical ion-exchange step occurs prior to traditional electrochemical transformation of the probe at the electrode–solution interface (47,64,66,68,69,76,78,151). While intrazeolite electron transfer was suggested for non-size-excluded redox probes (70,71), no unequivocal demonstration was provided for this, except when using appropriate spatially arranged mediators [Eqs. (4) and (5)] (56,57,178). Note that intrazeolite mass transport processes (i.e., site-to-site diffusion from small to large cages) may influence extracrystalline electron transfer.
2. Encapsulated complexes that are physically trapped in the zeolite pore structure and are therefore experiencing high steric constraints. These are amenable to electron transfer if located in the boundary region of the zeolite grains. An important question is the exact nature of these species situated in the outermost layers of the zeolite grains, which are considered either as extrazeolitic [Eq. (3a)] or intrazeolitic [Eq. (1)] depending on the authors (9,11,25,26). This leads to a large amount of electrochemically silent species (those located in the bulk zeolite, i.e., 98–99%), which can be slightly but not dramatically improved by the use of adsorbed mediators [Eqs. (5a) and (5b)].

These conclusions are upheld by the representative fundamental investigations illustrated above (Figs. 5–20), and the reader interested in more detail is directed to the abundant literature treating, at least in part, the question of the electron transfer mechanisms at ZMEs (9,11,17,20,24,47,66–71,76,78,79,84,87,89,109,119,120,122,123,127,151,159).

C. Compilation of the Electroactive Probes and Zeolite Types Investigated at ZMEs

Table 2 presents a compilation of most electroactive species and zeolites that have been studied by means of ZMEs. Electroactive probes can be classified into three categories: metallic species, organic species, and encapsulated organometallic complexes. The most frequently studied probes are Ag^{I}, Cu^{II}, methyl viologen, and metal-bipyridine and metal(salen) complexes, which consequently constitute the main illustrations depicted in this chapter. The most popular zeolites used to build ZMEs are the synthetic molecular sieves of type A, X, and Y, with a marked preference for zeolite Y, for two main reasons: its large-channel network provides high diffusion rates to the small non-size-excluded cations, and electroactive complexes can be encapsulated in its supercages.

Table 2 Electroactive Probes and Zeolites Studied at ZMEs

Electroactive probes[a]	Zeolite types	ZME configurations[b]	Ref.
A. Metal ions			
Ag^{I}	A	Zeolite-polymer film	63, 65, 70, 73, 76, 90, 193
	Faujasite (Y, X)	Zeolite-polymer film	66, 69, 73, 78, 83
		Zeolite-carbon-polymer film	94, 104
	Mordenite	Pressed "zeolite + carbon"	43, 179
	A, X, Y	ZMCPE	73, 171
Cu^{II}	Faujasite (Y, X)	Zeolite-polymer film	48, 64, 67, 68, 73, 92
	A, Y, modernite	Zeolite-carbon-polymer film	24, 94
	A, X, Y, mordenite, clinoptilolite	ZMCPE	48, 73, 148, 160, 167, 171
Hg^{II}, Ru^{III}	Y or natural	ZMCPE	48, 60, 159, 175
Fe^{II}, Co^{II}, Pb^{II}, Cd^{II}	Y	Zeolite-polymer film	58, 61, 62, 64, 91, 93, 200
Framework V	V-silicalite, VAPO-5	"zeolite + carbon" composites	107, 125, 126
Framework Ti	Titanosilicalite	ZMCPE or zeolite film	88, 149, 153
Co^{II}, Pb^{II}, Cd^{II}, U^{VI}	A, Y	Pressed zeolite pellet	129, 130
Cd^{II}, Na^{I}, Ag^{I}	A	Pressed zeolite pellet	38–40
B. Organic Species			
Methyl viologen	Y	Zeolite-polymer film	47, 57, 71, 73, 86, 89
		ZMCPE	73, 147, 150, 151, 154, 164, 169, 170, 106
	A, X, Y	ZMCPE	47, 73
Aromatic alcohols (hydroquinone, catechol, dopamine, phenol, etc.)	Faujasite (Y, X), zeolite mixture	ZMCPE, zeolite-polymer film	73, 85, 156, 162, 172
		Pressed "zeolite + carbon"	152
C. Organometallic complexes			
Metal-*tris*-bipyridine	Y	Zeolite-(carbon)-polymer film	24, 56, 79, 109, 194
		Pressed "zeolite + carbon"	114, 127
Metal-(salen)	Y	Zeolite-(carbon)-polymer film	24, 87, 109
		Pressed "zeolite + carbon"	113, 115–117, 119, 121
		Dispersed zeolites	185
Metal-phtalocyanines	Faujasite (Y, X)	Pressed "zeolite + carbon"	112, 118, 122, 123
Metal-porphyrins	Y, ZSM-5, EMC-2, VPI-5	Pressed "zeolite + carbon"	45, 120

[a]Abbreviation: salen = *N*,*N*′-bis(salicylidene)ethylenediamine.

[b]Zeolite-polymer film includes both composite films and zeolite layers covered with a polymer coating; zeolite-carbon-polymer film includes both composite films and "zeolite + carbon" layers covered with a polymer coating; pressed "zeolite + carbon" mixtures are casted on a metallic grid; ZMCPE: zeolite-modified carbon paste electrode, including zeolite-carbon-copolymer composites.

V. ADVANCED ELECTROCHEMICAL APPLICATIONS OF ZEOLITES

Fundamental studies to characterize the electrochemical behavior of ZMEs have revealed several aspects of confinement effects and/or ion-exchange properties of redox solutes in zeolite molecular sieves that arise from the combination of zeolites with an electrode–solution interface. It is now time to move beyond the basic knowledge and to demonstrate that the attractive zeolite properties can be readily exploited in practical applications. Most applied benefits of intersecting zeolite chemistry and electrochemical science have been achieved in two main fields: electroanalysis and electrocatalysis (9,10,12,13,17,18).

A. Electrocatalysis at Zeolite-Modified Electrodes

The electrochemical activity of either ion-exchanged species or encapsulated complexes in zeolites has been exploited in catalytic transformations. Examples of electrocatalysis involving ZMEs are available in the fields of organic chemistry (electro-assisted oxidation or reduction of organic substrates) and analytical chemistry (to improve sensitivity or selectivity of a particular electrochemical detection in the presence of a supported catalyst).

Zeolite-encapsulated metal complexes have found useful applications in the area of heterogeneous oxidation catalysis by taking advantage of the physical entrapment of catalysts in microporous spaces of the zeolite (124). Most reactions are chemically induced, but some investigations involving the electrochemistry of ZMEs are also reported for either electro-assisted oxidation or reduction (108,113,115,124,185). An illustrative example, given in Fig. 21, deals with the catalytic reduction of benzyl bromide (denoted as RX hereafter) by cyclic voltammetry in acetonitrile using a ZME of encapsulated Co(salen)-NaY zeolite (113). Enhancement of peak current for the Co^{II}/Co^{I} process and the concomitant disappearance of the Co^{I}/Co^{II} anodic signal indicate that the $[Co^{I}(salen)]^{-}$ complex [formed at about -1.3 V; Eq. (6a)] reacts with RX in a chemical redox step to give an $[RCo^{III}(salen)]$ intermediate [Eq. (6b)]. This is, at such a negative potential, directly reduced to regenerate the intermediate catalyst and the final product R^{-} [Eq. (6c)]. Continuous consumption of the $[Co^{I}(salen)]^{-}$ complex by reaction with RX makes the Co^{II}/Co^{I} process irreversible (Fig. 21).

$$[Co^{II}(salen)] + 1e^{-} \Rightarrow [Co^{I}(salen)]^{-} \qquad (E \approx -1.3V) \tag{6a}$$

$$[Co^{I}(salen)]^{-} + R^{+} \Rightarrow [RCo^{III}(salen)] \tag{6b}$$

$$[RCo^{III}(salen)] + 2e^{-} \Rightarrow [Co^{I}(salen)]^{-} + R^{-} \quad (E' \text{ less cathodic than } -1.3 \text{ V}) \tag{6c}$$

The electrocatalytic activity of Co(salen)-NaY was also studied as a microheterogeneous dispersion undergoing controlled potential electrolysis at a high-surface-area reticulated vitreous carbon electrode (see experimental device in Fig. 4). The importance of the zeolitic environment on the reactivity of the electrogenerated $[Co^{I}(salen)]^{-}$ complex to catalyze the reaction of benzyl chloride with CO_2 was demonstrated by comparison of Co(salen)-NaY to homogeneous Co(salen): higher electrocatalytic turnover (1000-fold increase) and longer durability (200%) were obtained with the encapsulated catalyst (185). Such improvements are attributed to the particular physicochemical environment of the zeolite and site isolation experienced by the Co(salen) complex.

A similar electro-assisted reaction was observed for the reduction of dioxygen in acetonitrile using Mn(salen) encapsulated in zeolite Y, which gives an Mn^{III}-superoxo

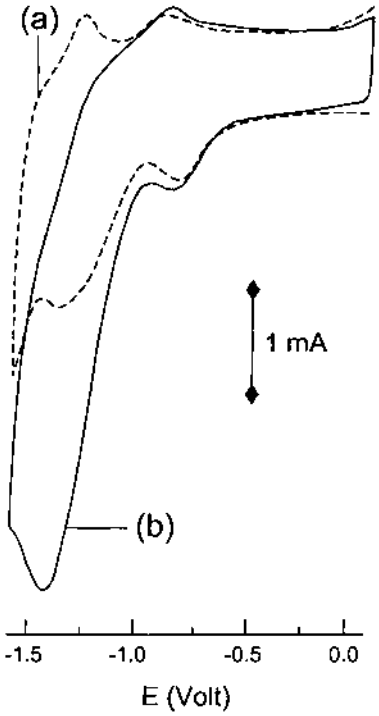

Fig. 21 Cyclic voltammograms of pressed powder graphite-Co(salen)-NaY electrode in (a) acetonitrile + 0.1 M tetrabutylammonium tetrafluoroborate solution, and (b) the same solution as (a) containing 5 mM benzylbromide in addition. Potential scan rate, 10 mV/s. (Adapted from Ref. 113, with permission.)

complex in the presence of cocatalyst 1-methylimidazole; such promoted dioxygen activation can be applied to the biomimetic hydrocarbon oxidation process (115). Electrocatalytic reduction of oxygen was also achieved by voltammetric induction at ZME containing iron phthalocyanine trapped in zeolite Y (FePcY) (108). In addition, the same electrocatalyst was found to catalyze the oxidation of hydrazine with better performance than FePc supported on a titanium oxide–coated, silica gel–modified electrode (108,201).

Zeolite-supported electrocatalysts can be exploited to improve the performance of analytical sensing devices. The electroanalytical applications of ZMEs dealing with electrocatalytic processes are summarized in Table 3. Two actions of the catalyst are (a) enhancement of the peak current intensity by continuous electrogeneration-consumption of the active intermediate, and (b) lowering of the target analyte overpotential.*

An example of the first case is illustrated in Fig. 22, where peak height relative to the electrochemical oxidation of ascorbic acid is significantly more intense when recorded at a

*The term *overpotential* is related to a shift in the potential giving rise to significant oxidation (reduction) of a target analyte at a more positive (negative) value than the thermodynamic formal potential characteristic of the redox couple. Overpotentials are caused by limited kinetics of the electron transfer, which can make the electrochemical transformation more difficult (188).

Table 3 Electroanalytical Applications of Zeolite-Modified Electrodes: Electrocatalysis

Analyte	Zeolite[a]	Electrode[b]	Medium[c]	Regeneration	Method[d]	Concentration range	Detection limit	Ref.
Ascorbic acid	Fe^{III}-Y	Zeolite/graphite/PS coating on GC	Phosphate buffer (pH 6.8)		CV, A	1.6×10^{-6}–2.1×10^{-2} M		105
Ascorbic acid	Fe^{III}-Y	Zeolite-modified CP	Aqueous KCl (pH 7)	Mechanical	CV	Up to 10^{-3} M	4×10^{-6} M	161
Dopamine, norepinephrine	TP^{+}-Y	Zeolite-polymer film on solid electrode	Phosphate buffer (pH 7)		DPV	10^{-6}–10^{-4} M		85
Gaseous ethanol and ammonia	Na-Y	Gold deposit on a pressed zeolite pellet	Gaseous N_2		CV	C_2H_5OH: 11.5–40 torr NH_3:30–126 torr		143
Hydrazine	Y	Zeolite-CuTPP-modified CP	0.5 M $NaClO_4$ (pH 7)		CV, A	2×10^{-7}–1×10^{-6} M	1×10^{-7} M	165
4-Nitrophenol	Zeolite mixture	Zeolite-modified CP	BR buffer (pH 3.5)	Mechanical	DPV	0.2–10 mg l^{-1}	0.04 mg l^{-1}	172
O_2 (dissolved)	Na-A, Na-Y	Zeolite-modified CP	Aqueous $LiClO_4$ and $MVCl_2$		CV			147
O_2 (dissolved)	L	Zeolite-modified BPG/poly(phenosafranine)	0.1 M NaH_2PO_4		CV, LSV-RDE			95

[a]Abbreviation: TP+, 2,4,6-triphenylpyrylium.
[b]Abbreviations: PS, polystyrene; GC, glassy carbon; CP, carbon paste; CuTPP, copper-tetraphenylporphyrin; BPG/poly(phenosafranine), phenosafranine electropolymerized on basal plane graphite.
[c]Abbreviations: BR, Britton-Robinson; $MVCl_2$, methyl viologen dichloride.
[d]Abbreviations: CV, cyclic voltammetry; A, amperometry; LSV-RDE, linear scan voltammetry–rotating disk electrode.

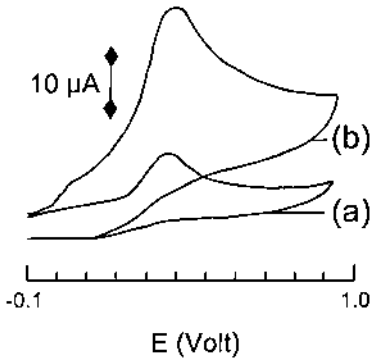

Fig. 22 Cyclic voltammograms of ascorbic acid (1.0×10^{-3} M) at (a) unmodified glassy carbon electrode and (b) zeolite Fe^{III}-Y-modified glassy carbon electrode, recorded in 0.1 M Na_2SO_4. (Adapted from Ref. 105, with permission.)

Fe^{III}-Y zeolite–modified electrode in comparison with the corresponding unmodified glassy carbon. This improvement, due to the mediated oxidation of the analyte by electrogenerated Fe^{II} species, leads to more sensitive detection of ascorbic acid and was applied to analysis of fruit samples (105). Similar enhancement of the voltammetric signals was obtained for the detection of hydrazine by means of ZME containing a copper-porphyrin, for which a fast response time was observed in amperometry by attaining a stable maximal current in less than 1 s (165). Zeolite Y–modified carbon paste ion exchanged with methyl viologen was applied to the reduction of dissolved oxygen, which is promoted by electrogeneration of the methyl viologen radical cation. After optimization by the simplex method, maximal catalytic currents were obtained using an electrode containing 49% (w w) zeolite immersed in 32 mM methyl viologen (that readily accumulates within zeolite Y) saturated with oxygen, with an equilibration period of 46 min (147).

Examples of the second case (lowering overpotentials with ZMEs) are also available. Electrochemical oxidation of aromatic alcohols, e.g. nitrophenols (172) or hydroquinone (152), is facilitated at ZME; the zeolite probably aids in the removal of protons (associated with the oxidation process), similar to the process observed with alumina or layered double hydroxides (175). Electrocatalytic reduction of oxygen was also achieved at zeolite/poly(phenosafranine) electrodes, lowering the reduction potential by 300 mV with respect to a corresponding unmodified electrode, where the zeolite (type L) acted to improve the reversibility of the poly(phenosafranine) catalyst (95). Finally, pressed zeolite pellets were used as a support for high surface area gold deposits, which were then applied to the catalytic detection of ethanol and ammonia vapors (143). Other cases of electrocatalysis are presented in Sec. V.D.

B. Preconcentration and Permselectivity

Sensitivity increases and lower detection limits can be achieved in electrochemistry by applying a chemical preconcentration step prior to the voltammetric quantification. At chemically modified electrodes, a judicious choice of the modifier may also improve selectivity by specific binding of the target analyte to the modifying agent. The general principle of preconcentration analysis usually involves four steps, as illustrated in Fig. 23. In the first step, an electrode is maintained at open circuit (without applying any electrical stimuli) in a stirred solution containing the target analyte, for a certain period of time, to

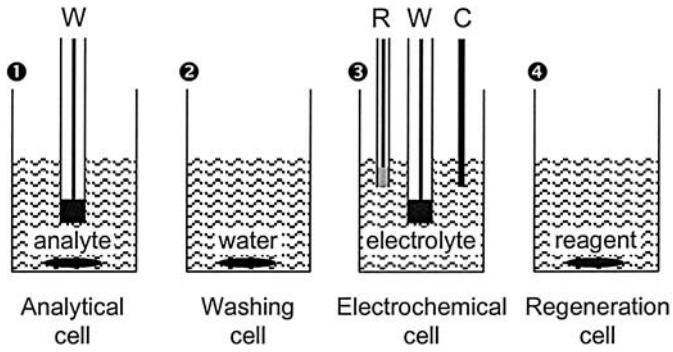

Fig. 23 Schematic representation of the successive steps applied in preconcentration analysis involving electrochemical detection. R is the reference electrode, W the working electrode, and C the counterelectrodes.

ensure accumulation of the analyte in and on the electrode modifier in contact with the solution. After rinsing the electrode in pure water in the second step, the third step involves transfer of the modified electrode into an electrochemical cell containing an appropriate electrolyte in order to quantify the previously accumulated species (this could require desorption of the analyte). A fourth step is then often necessary to perform successive analyses, i.e., regeneration of the electrode surface, which is achieved by treatment into a stirred solution containing an adequate reagent.

With ZMEs, the accumulation proceeds via ion exchange of a cationic electroactive analyte in the zeolite particles located at the electrode surface. Regeneration might be achieved by the reverse exchange by immersing the electrode in a solution containing the initial zeolite cocation (most often Na^+). These ion-exchange reactions are intrinsically simple, but their implementation may become intricate because of impregnation of solutions deep in the bulk electrode structure (leading to memory effects). One can imagine this from the various ZME devices comprising free spaces (Figs. 1–3), as was demonstrated experimentally for the zeolite-modified carbon paste electrode (150). To circumvent these memory effects, mechanical renewal of the electrode surface was applied (73,156,169) or, as an alternative, one group resorted to screen-printed ZMEs (170). The electroanalytical applications of ZMEs operating in the preconcentration mode are described in Table 4.

A natural zeolite from volcanic rocks in the Canary Islands was mixed in carbon paste to sense mercury(II) species (46). Zeolite A was chosen for the accumulation of silver(I) prior to its quantification by differential pulse voltammetry; good selectivity was observed toward other metal species because of the high affinity of zeolite A for silver(I) (146). The influence of both the zeolite type (A, X, Y) and ZME device (bulk zeolite-modified carbon paste, or zeolite monograin coated on glassy carbon) on the analysis of silver(I), copper(II), dopamine, and methyl viologen was investigated (73). Highest sensitivities and lowest detection limits were obtained with zeolites displaying the largest pores, highest capacity, and smallest particle size because such conditions enable fast mass transport and therefore high accumulation efficiency. The bulk ZME usually gives faster response time than film-based electrodes because the latter induce diffusional limitations brought about by the hydrophobic polymer film acting as a screening barrier to the aqueous solutions. The addition of ammonia in the detection medium leads to improved signals for copper(II) because of more efficient desorption

Table 4 Electroanalytical Applications of Zeolite-Modified Electrodes: Preconcentration and Permselectivity

Analyte[a]	Zeolite	Electrode[c]	Medium	Regeneration	Method[d]	Concentration range	Detection limit	Ref.
Ag^{+}	Na-A	Zeolite-modified CP	Aqueous $NaNO_3$	Chemical + electrochemical	Accumulation (o.c.) + DPV	0.5–5 mg l^{-1}	0.08 mg l^{-1}	146
Cu^{2+}	Na-A, Na-X, Na-Y	Zeolite-modified CP, zeolite monograin on GC	Aqueous $NaNO_3$	Mechanical or chemical	Accumulation (o.c.) + CV	5×10^{-5}–1×10^{-3} M		73, 163
Cu^{2+}	K-A, Na-A, Ca-A, Na-X	Zeolite-modified CP	Phosphate buffer (pH 4.2)	Chemical	Accumulation (o.c.) + SWV	0.3–1.0 mg l^{-1}	74 μg l^{-1}	160
Cu^{2+}, Cd^{2+}, Zn^{2+}	K-A, Na-A, Ca-A, Na-X	Zeolite-modified CP	Phosphate (pH 6) or ammonia (pH 9) buffers	Chemical	Cathodic deposition + SWV	0.3–1 ppm (Cu^{2+}) 0.2–2 ppm (Cd^{2+}) 0.2–1.2 ppm (Zn^{2+})	300 nM 87 nM 145 nM	157
Dopamine, epinephrine	Na-Y	Zeolite-modified CP	Phosphate buffer	Mechanical or chemical	DPV or FIA	2×10^{-5}–1×10^{-3} M		156
Hg^{2+}	Natural[b]	Zeolite-modified CP	Aqueous KNO_3	Chemical	Accumulation (o.c.) + CV	0.11–2.2 mg l^{-1}		46
Methyl viologen	Na-Y	Zeolite-modified CP	Water	Mechanical or chemical	Accumulation (o.c.) + CV	5×10^{-5}–5×10^{-3} M		169
Paraquat, diquat	Na-Y	Zeolite-modified screen-printed electrode	Water	Chemical	Accumulation (o.c.) + SWV	1×10^{-6}–1×10^{-5} M	$< 1 \times 10^{-7}$ M	170
Zn^{2+}	Na-X	Zeolite + PS coating on GC covered with Hg	Aqueous KNO_3		Cathodic deposition + SWV	5×10^{-7}–3.5×10^{-6} M[e]		77

[a]Abbreviation: Methyl viologen, *N*,*N*′-dimethyl-4,4′-bipyridinium.
[b]From volcanic rocks (Canary Islands).
[c]Abbreviations: CP, carbon paste; GC, glassy carbon; PS, polystyrene.
[d]Abbreviations: o.c., open circuit; DPV, differential pulse voltammetry; CV, cyclic voltammetry; SWV, square wave voltammetry; FIA, flow injection analysis.
[e]In the presence of 10 μM Cu^{2+}.

of the analyte out of the zeolite, as helped by complexation with NH_3 ligands (160). Other metal species such as Cd^{II} and Zn^{II} were also detected after preconcentration at ZMEs (77,157).

An interesting result is the restricted interference of Cu^{II} in the determination of Zn^{II} by anodic stripping voltammetry, achieved when using a zeolite X–polymer film coated on glassy carbon and covered by an electrodeposited mercury film (77). In this case, the well-known intermetallic Zn/Cu compound that is formed in great quantities during electrolytic deposition of Zn^{2+} in the presence of Cu^{2+} at a conventional mercury electrode was produced in a much smaller amount, and its stripping peak was not as close to that of Zn. The ability of the zeolite to trap Cu^{2+} species during zinc deposition makes ZME suitable for discriminating Cu^{2+} in the stripping determination of Zn^{2+}.

Organic species such as the pesticides paraquat (methyl viologen) and diquat (170), or the neurotransmitters dopamine and epinephrine (156), can be accumulated by ion exchange in zeolites prior to their electrochemical detection. Practical utility of ZME for field sensing was illustrated for the detection of paraquat at single-use zeolite-modified carbon electrodes (170). As shown in Fig. 24, the response time of the thick-film composite electrode is much faster than the corresponding zeolite-modified carbon paste sensor, with a maximal preconcentration level reached in just 3 min. This circumvents the memory effects usually encountered with ZMEs after prolonged exposure to the external solution. Another interesting feature of zeolites is their charge selectivity property. It was exploited at ZMEs for the permselective detection of positively charged neurotransmitters in the presence of ascorbic acid, a common interference in the detection of dopamine or epinephrine. Total selectivity for the neurotransmitters over ascorbic acid was obtained using a zeolite Y–modified carbon paste electrode in flow injection analysis for which the potential scan was applied with a delay time after the injection of the analyte sample. During this time, positively charged dopamine or epinephrine was accumulated

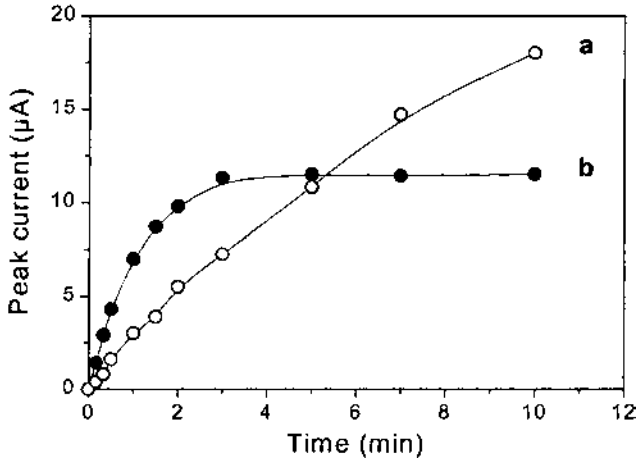

Fig. 24 Peak current response for the uptake of 1.0×10^{-6} M paraquat in two zeolite Y–modified electrodes, as a function of the accumulation time. (a) Zeolite-modified carbon paste electrode, and (b) zeolite-modified screen-printed electrode. Detection was performed in 0.1 M NaCl, by square wave voltammetry (with a 100-Hz frequency, a 5-mV step height, and a 50-mV modulation amplitude). (Adapted from Ref. 170, with permission.)

by ion exchange while ascorbic acid (neutral or even slightly negative at the physiological pH) was rejected by the zeolite. Ascorbic acid was therefore flowing far from the electrode surface, and a voltammetric peak for only the target neurotransmitter was observed (156).

C. Indirect Amperometric Detection

Zeolites present definite advantages over other ion exchangers because they combine, in a single material, both ion-exchange and size selectivity properties. This combination has generated what is (in this author's opinion) one of the most elegant electroanalytical applications of ZMEs: the indirect amperometric detection of species that cannot usually be detected by amperometry.

Let us consider the case of potassium ion. K^+ cannot be reduced in aqueous medium at a conventional electrode surface because this process would occur at more negative potentials than that corresponding to water reduction. But when using a ZME doped with an appropriate charge transfer mediator, K^+ can be indirectly detected by amperometry in aqueous medium containing a size-excluded electrolyte cation. The principle is illustrated in Fig. 25 and described by the following equations:

$$E^{m+}_{(Z)} + mTBA^{+}_{(S)} \neq E^{m+}_{(S)} + nTBA^{+}_{(Z)} \tag{7}$$

$$E^{m+}_{(Z)} + mK^{+}_{(S)} \Leftrightarrow E^{m+}_{(S)} + mK^{+}_{(Z)} \tag{8a}$$

$$E^{m+}_{(S)} + ne^{-} \Leftrightarrow E^{(m-n)+}_{(S)} \tag{8b}$$

where the subscripts Z and S refer to the zeolite phase and the solution, respectively.

Immersing a ZME exchanged with an electroactive species (E^{m+}, i.e., Cu^{2+} in Fig. 24) in an electrolyte solution of which the cation is too large to enter the zeolite framework (i.e., tetrabutylammonium, TBA^+) does not result in any redox behavior because charge balance cannot be maintained [Eq. (7)]. Electrolytes with size-excluded cations are thus electrochemically inert and serve as the supporting electrolyte that ensures ionic conductivity, which is required in most electrochemical experiments. But anytime that a solution containing a certain amount of non-size-excluded cation (e.g., K^+) is brought in contact with a zeolite particle located at the electrode surface, an equivalent amount of E^{m+} species (i.e., Cu^{2+} in Fig. 25) can be liberated by ion exchange [Eq. (8a)] and can be detected amperometrically at the electrode surface [Eq. (8b)]. The current signal is due to the reduction of the mediator, but its intensity is directly monitored by the concentration of the K^+ sample. As such, this corresponds to the indirect amperometric detection of the usually nonelectroactive potassium species. ZMEs exchanged with an electroactive mediator therefore act as amperometric sensors for nonelectroactive non-size-excluded cations. This is illustrated in Fig. 26 where the flow injection analysis of K^+ samples at a Cu^{2+}-Y-ZME gives rise to amperometric signals directly proportional to the analyte concentration in the 0.05- to 0.5-mM range, in both the increasing and decreasing concentration directions (167). This demonstrates the combination of both ion-exchange capacity and size selectivity of zeolites in the amperometric sensing principle. It was largely developed by the Baker's group (64,67,94,193,202,203), as well as by Walcarius and coworkers (154,164,167,168,171).

Silver(I)-exchanged faujasites and mordenite were applied to the analysis of alkali metal cations in organic and hydroorganic media in the ppm concentration range (64,67,

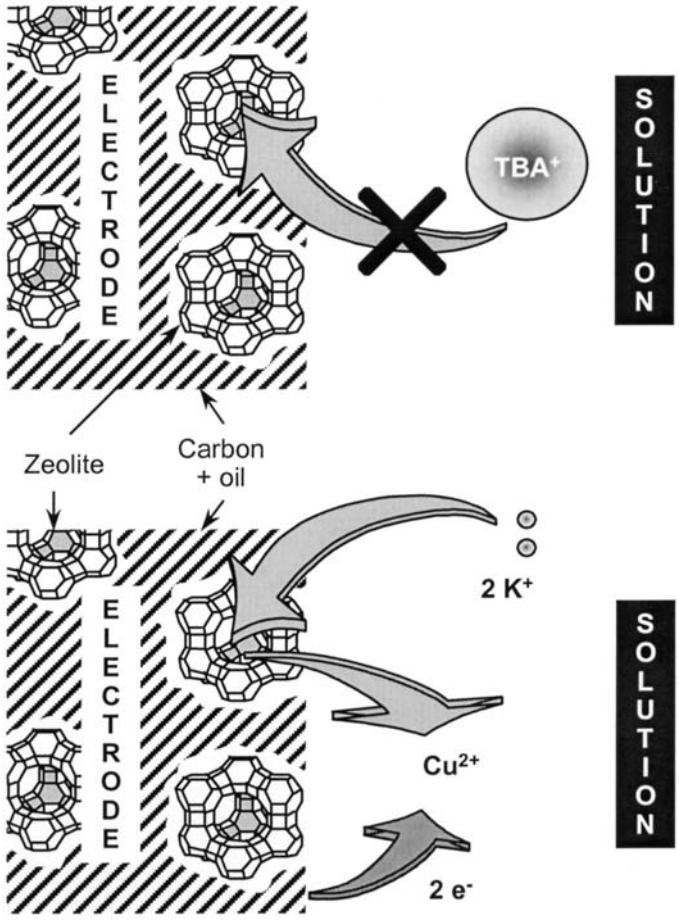

Fig. 25 Schematic representation of the detection principle for the indirect amperometry at the copper-doped zeolite–modified carbon paste electrode (the case of K^+). (Reprinted from Ref. 167, with permission.)

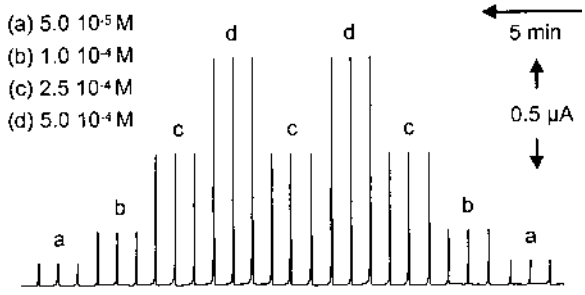

Fig. 26 Continuous injections of (a) 5.0×10^{-5} M, (b) 1.0×10^{-4} M, (c) 2.5×10^{-4} M, and (d) 5.0×10^{-4} M K^+ samples (into 10^{-2} M tetrabutylammonium bromide): flow injection analysis responses of a copper-doped zeolite modified carbon paste electrode; carrier, 10^{-2} M tetrabutylammonium bromide; flow rate, 5 ml/min; applied potential, −0.25 V. (Reprinted from Ref. 167, with permission.)

94,193). The amperometric signals are monitored by the amount of Ag^+ that is released from the zeolite by ion exchange with the cationic analyte. Therefore, the peak height is proportional to the concentration of alkali metal cations (similar to Fig. 26), in a range depending on the analyte (Table 5), and the amperometric intensity is directly related to the speed of the Ag^+–cationic analyte exchange. For zeolites containing Ag^+ species located mainly in the large cages, the selectivity series was $Cs^+ > K^+ > Na^+ > Li^+$. According to the size of hydrated cations, the smaller analytes gave the higher signals. This was the case of Ag-Y and Ag-mordenite (67,94,193). On the other hand, the zeolite Ag-X that contains more Ag^+ in the small cages had the highest sensitivity for K^+, with currents decreasing according to $K^+ > Na^+ > Cs^+ \sim Li^+$ (67). This series arises from two components acting in opposite directions on the electrode response: ion exchange of the mediator located in the large cages, which is controlled by the hydrated radii of the cationic sample, and those located in the small cages for which the exchange is depending on solvation energies and ionic radii of cations (137). The ammonium series was also investigated in water-methanol mixtures using Ag-Y zeolite (64) or in pure water using MV-Y zeolite (154,164), giving a response decreasing as follows: ammonium > tetramethylammonium > tetraethylammonium tetrapropylammonium. This is in agreement with the size of the analytes.

Indirect amperometric detection at ZME was applied in aqueous medium for the analysis of alkali metal, alkaline earth, and ammonium ions in both batch and flow injection modes, using methyl viologen or copper(II) as the mediator and various zeolite types (154,167,168). In every case, the electrode response increased with charge of the positive ion and as the hydrated ion size decreased. Therefore, the mediators contributing effectively to the electrochemical signal are mainly or exclusively those located in the large channel network of the zeolite. The selectivity series Ca^{2+}, Mg^{2+}, $Cs^+ > K^+ > Na^+$, $NH_4^+ > Li^+$ is unaffected by the nature of the zeolite used (167). Even when using the NH_4^+-selective clinoptilolite (doped with Cu^{2+}), no significant increase in peak current for NH_4^+ was observed with respect to other cations (168). This confirms that the indirect detection process [Eq. (8b)] is controlled mainly by kinetics associated with ion exchange [Eq. (8a)], and thus by diffusion in the zeolite lattice, rather than by the thermodynamics relative to the affinity of the zeolite for one cation or another. This is further confirmed by the effect of pore aperture and particle size of zeolites on the amperometric response: peak heights increase with "openness" of the zeolite structure and with decrease in the particle size (167). In addition, the use of the more mobile Ag^+ mediator, instead of Cu^{2+}, resulted in a twofold enhancement of peak currents (171).

Additional electroanalytical applications of indirect amperometric detection at ZME have been derived from solvent effects that were observed from voltammetric studies of electroactive species exchanged in zeolites (see Sec. IV.A.2 of this chapter). For example, peak currents recorded for AgA in pure dimethylformamide (DMF) containing a non-size-excluded electrolyte ($LiClO_4$) are several hundred times smaller than in water because nonaqueous ion exchange occurs slowly in contrast to fast ion exchange in water (63). Figure 27 shows that gradual addition of water (in the ppm range) to dry DMF + $LiClO_4$ results in a proportional increase in peak currents sampled by anodic stripping voltammetry at an AgA-modified electrode. This electrode is thus a sensor for trace water in organic solvents containing a small amount of alkali metal cation (202,203), with a linear response in the 1- to 10-ppm concentration range and a detection limit close to 20 ppb (63,193), which is by far better than the classical Karl Fischer method. An experimental setup based on this detection scheme, which displays a long useful lifetime, was recently designed by coupling a zeolite AgA column to a classical thin-layer electrochemical cell (193). This

Table 5 Electroanalytical Applications of Zeolite Modified Electrodes: Indirect Amperometric Detection

Analyte[a]	Zeolite[b]	Electrode[c]	Medium[d]	Regeneration	Method[e]	Concentration range	Detection limit	Ref.
Alkali-metal ions	Ag-Y	Zeolite/graphite/PS coating on ITO	DMF, CH_3CN, MeOH (+TBAP)		Reduction + ASV	1–10 ppm (Li^+) 1–35 ppm (Na^+) 1–25 ppm (K^+)	< 1 ppm	94
Alkali-metal ions, NH_4^+, TMA^+, TEA^+, TPA^+	Ag-X, Ag-Y, Ag-mordenite	Zeolite/graphite/PS coating on ITO	MeOH/water (+TBAP)		CV (reduction)	1×10^{-4}–1×10^{-3} M		64, 67, 193
Alkali metal, alkaline earth, NH_4^+ ions	MV-Y	Zeolite-modified CP	Aqueous TBABr	Mechanical or chemical	A (reduction) BIA, FIA	1×10^{-3}–1 M	1×10^{-4} M	154, 164
Alkali metal, alkaline earth, NH_4^+ ions	Cu-A, Cu-X, Cu-Y, Cu-clinoptilolite	Zeolite-modified CP	Aqueous TBABr	Chemical	A (reduction) FIA	5×10^{-6}–5×10^{-4} M	4×10^{-7}–2×10^{-6} M[f]	167
Alkali metal, alkaline earth, NH_4^+ ions	Cu-A, Cu-X, Cu-Y, Ag-A, Ag-X, Ag-Y	Zeolite-modified CP	Pure water (without added electrolyte)	Chemical	A (reduction) FIA, IC	5×10^{-6}–5×10^{-4} M	5×10^{-7}–2×10^{-6} M[f]	171
Ammonium ions	Cu-clinoptilolite	Zeolite-modified CP	Aqueous TBABr	Chemical	A (reduction) FIA	2×10^{-5}–1×10^{-3} M	5×10^{-6} M	168
Benzene, trichloro-ethylene	Ag-A	Zeolite/graphite/PS coating on ITO or RVC	Aqueous medium		Reduction + DPASV or FIA	20–100 ppm		193
H_2O	Ag-A	Zeolite/graphite/PS coating on ITO	DMF, $LiClO_4$		Reduction + ASV	1–10 ppm	20 ppb	63, 193
TMA^+	Silicalite	Zeolite layer grown on Hg	Water/dichloro-ethane interface		Polarization of ITIES			111

[a]Abbreviations: TMA^+, tetramethylammonium; TEA^+, tetraethylammonium; TPA^+, tetrapropylammonium.

[b]Abbreviation: MV-Y, methyl viologen-exchanged zeolite Y.

[c]Abbreviations: PS, polystyrene; ITO, indium tin oxide; CP, carbon paste; RVC, reticulated vitreous carbon.

[d]Abbreviations: DMF, dimethylformamide; CH_3CN, acetonitrile; MeOH, methanol; TBAP, tetrabutylammonium perchlorate; TBABr, tetrabutylammonium bromide.

[e]Abbreviations: ASV, anodic stripping voltammetry; CV, cyclic voltammetry; A, amperometry; BIA, batch injection analysis; FIA, flow injection analysis; IC, ion chromatography; DPASV, differential pulse anodic stripping voltammetry; ITIES, interface between two immiscible electrolyte solutions.

[f]Depending on the cationic analyte (for Cu-Y).

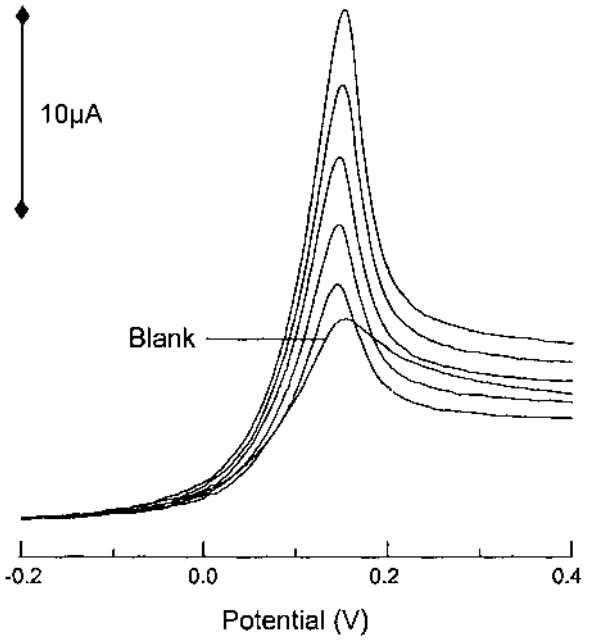

Fig. 27 Anodic stripping voltammograms of Ag^+-exchanged zeolite A in dry dimethylformamide with 0.1 M $LiClO_4$. Water added to the blank in ppm increments. Scan rate, 20 mV/s. Potential measured against a Pt quasi-reference electrode. (Reprinted from Ref. 63, with permission.)

approach is more suited to routine analysis than ZME and allows in situ regeneration of the zeolite particles by a simple flow of silver(I) solution through the zeolite column. Alternatively, trace organic solvents in freshwater can be detected by using zeolites having a multiple cage structure and containing an electroactive mediator (i.e., Ag^+ ions) in its small channels (193,204,205). In this case, the electrochemistry of silver (or other mediator) is somewhat hindered because it requires the rather slow intrazeolite diffusion of Ag^+ from small to large cages and then to solution (see Sec. IV.A.2 and Fig. 10 of this chapter). This process can be facilitated when a molecule that complexes silver is present in solution (24). For example, in the presence of benzene the electrochemistry of $AgNH_4Y$ (with Ag^+ in the small cages and NH_4^+ in the supercages) was found to give higher response than in pure water since benzene is known to form a weak complex with silver and facilitates therefore its extraction from the small zeolite cages. This resulted in peak currents increasing with the benzene concentration (193).

Attempts were made to exploit the indirect amperometry at ZMEs for detection in ion chromatography (IC). A first try to get a novel suppressor-free detector in IC was carried out with methylviologen-exchanged zeolite Y and a mobile phase made of 0.05 M tetrabutyl-ammonium bromide (TBABr) (164). It was indeed possible to detect the alkali metal cations after being separated on an ion exchange column from the mixture "5 mM Li^+ + 5 mM Na^+ + 20 mM K^+ + 50 mM Cs^+" with a satisfactory fast response time. However, the unusual mobile phase (TBABr electrolyte), which is not well-suited to IC experiments, resulted in poor separations. The use of common mobile phases for the analysis of cations [most often solutions containing acids and/or small ions (206) is prevented here because the aluminium-rich zeolites are not stable in acid medium and

would therefore lose the mediator in the presence of protons. Overcoming this problem has led to the evaluation of ZME in the absence of supporting electrolyte, in order to determine whether the detector can be applied in IC working with conventional mobile phases and suppressor devices. Figure 28 shows that ZMEs give effective current responses upon injection of cationic analytes, and that they are even more sensitive than when recorded in the presence of TBABr. When using NaY zeolite, only small capacitive currents are observed, but the CuY gives rise to an additional component due to the reduction of Cu^{2+} upon ion exchange with the cationic analyte. The analyte plays two roles: as a transient electrolyte when sample is passing the electrode surface and as a source of faradic current by liberating the mediator that is detected amperometrically (171). The system is thus applicable to detection in IC after chemical suppression of the mobile phase electrolyte, as exemplified in Figure 29, which shows a satisfactory response of the copper(II)-doped ZME as similar to the conventional conductivity detector. The possible use of the modified electrode in the absence of added electrolyte opens the door to exploit other ion exchangers that do not necessarily display molecular sieving properties, such as polymeric resins, in designing indirect amperometric detection for IC (207).

Finally, another type of amperometric detection at ZME was recently proposed, based on the polarization of an interface between two immiscible electrolyte solutions (ITIES) modified by a zeolite membrane (111). Polarization of ITIES results in the observation of an electric current only when potential is sufficiently high (absolute value) to promote the crossing of the analyte from one phase to another (usually hydrophilic cations from aqueous to organic medium) (208,209). For example, crossing the unmodified water/1,2-dichloroethane liquid-liquid interface is favoured thermodynamically for tetraethylammonium (TEA) relative to tetramethylammonium (TMA). Figure 30 shows that modifying such an interface by a silicalite membrane results in the suppression of the electrochemically driven transfer of the TEA cation while still allowing the transfer of TMA, because of the molecular sieving effect of the zeolite membrane. This illustrates the

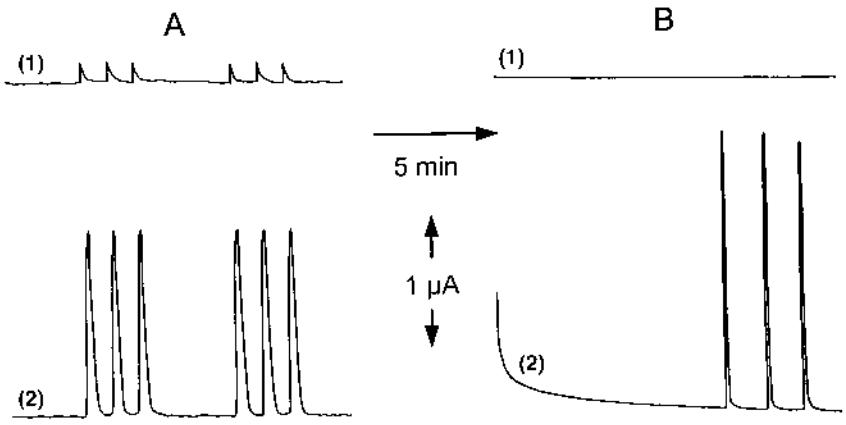

Fig. 28 Flow injection responses obtained at (1) an undoped zeolite Y–modified electrode and (2) a copper-exchanged zeolite Y–modified electrode. (A) Injection of 1.0×10^{-5} M Na^+ (in water); carrier, water; flow rate, 1.5 ml/min; applied potential, −0.4 V. (B) Injection of 1.0×10^{-3} M Na^+ (into 10^{-2} M tetrabutylammonium bromide); carrier, 10^{-2} M tetrabutylammonium bromide); flow rate, 5 ml/min; applied potential, −0.4 V. (From Ref. 171, with permission.)

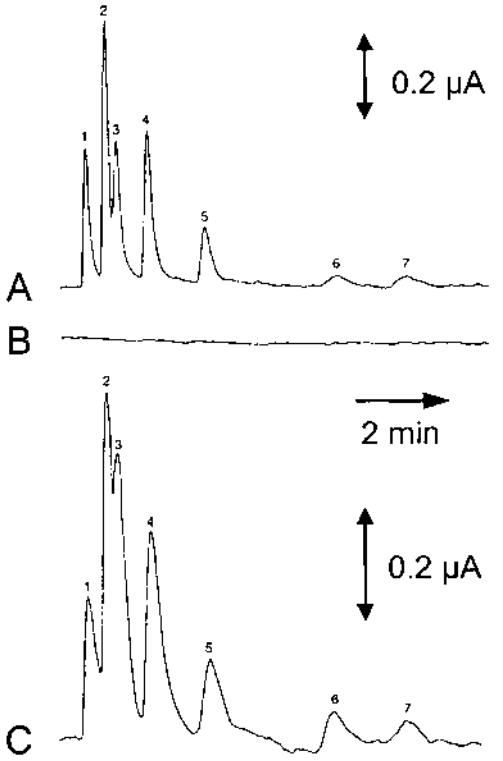

Fig. 29 Chromatograms obtained using (A) a classical conductivity detector, (B) a NaY zeolite–modified carbon paste electrode, and (C) a copper-exchanged zeolite Y–modified carbon paste electrode, for a standard mixture of cations: 0.7 mM Li^+ (1), 0.2 mM Na^+ (2), 0.3 mM NH_4^+ (3), 0.13 mM K^+ (4), 0.04 mM Cs^+ (5), 0.2 mM Mg^{2+} (6), and 0.13 mM Ca^{2+} (7); mobile phase, 3×10^{-3} M HNO_3 + 10^{-4} M EDTA; flow rate, 1 ml/min; applied potential [for (B) and (C)], −0.4 V. (From Ref. 171, with permission.)

possibility of zeolite rectification of electrochemical ion transfer by exploiting the size selectivity of zeolites (111).

D. Dispersion Electrolysis and Electrocatalysis at "Electrode-Modified Zeolites"

Charge-transfer reactions involving zeolite particles, modified with either redox solutes or nanocrystalline particles, which have been suspended in solution between feeder electrodes (see Fig. 4) have been widely studied and applied by Rolison and coworkers, as described in a recent account (13). One can distinguish two kinds of applications, both of them in the field of electrocatalysis: (a) dispersion electrolysis with metal (or metal oxide)–supported nanoelectrodes, and (b) electrochemically activated microheterogeneous catalysis involving zeolites in the transformation of organic compounds.

Template synthesis of nanoscale metal particles in and on the porous zeolite structure (210) is a common way to prepare supported nanocrystallites acting as ultramicroelectrodes (52). When dispersed in a solution between two feeder electrodes, they can be electrically charged upon polarization of the electrodes. Figure 31 illustrates that microheterogeneous dispersions of zeolite-supported Pt nanocrystallites (PtY) can effec-

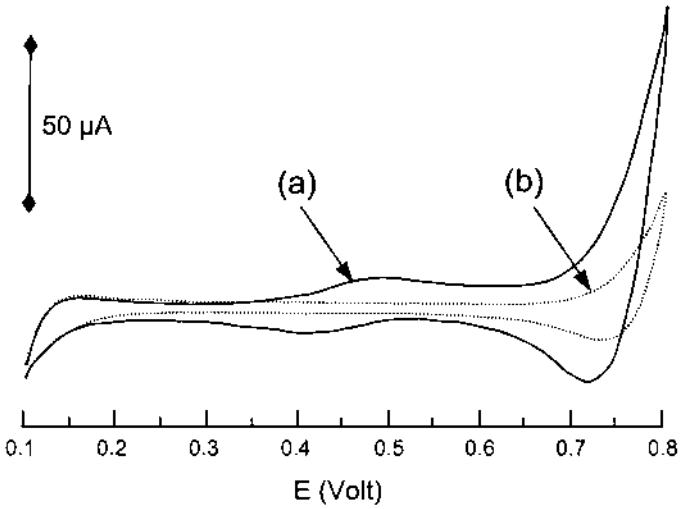

Fig. 30 The cyclic voltammetric response of the water|1,2-dichloroethane (DCE) interface using the cell {Ag(s)|AgCl(s)|BTPPA Cl (1 mM) + LiCl (0.012 M) (aq)|BTPPA TBP (0.021 M) (DCE) ‖ silicalite|Li_2SO_4 (0.020 M) + X + (aq)|Ag_2SO_4(s)|Ag(s)}, where BTPPA is bis(triphenylphosphornylidene)ammonium and TBP tetraphenylborate, with X = tetramethylammonium at an aqueous phase concentration of 0.83 mM (curve a) and X = tetraethylammonium at an aqueous phase concentration of 0.39 mM (curve b). The scan rate employed was 60 mV/s in both cases. (Reprinted from Ref. 111, with permission.)

tively electrolyze water in the absence of added electrolyte* when subjected to a dc voltage greater than 15 V/cm. No significant electrolysis occurs in the absence of dispersed PtY particles, while 1% Pt supported on γ-alumina or unsupported Pt microspheres gave rise to current densities one to two orders of magnitude lower than PtY (52,53,212). With zeolite-supported Pt, electrolysis occurs only at the boundary-site Pt particles, and the higher efficiency observed with the lower Pt contents (Fig. 31) was attributed to smaller size of the Pt nanocrystallites in the less loaded zeolites (53). It was also verified that water electrolysis was effectively due to the catalytic behavior of the Pt ultramicroelectrodes rather than an increase in the bulk solution conductivity that would occur upon zeolite-promoted autoprotolysis of water [which inevitably occurs when zeolite particles are immersed in pure water (41)]. This was achieved by electrolyzing a filtrate solution obtained after thorough contact with PtY particles: very low electrolysis efficiency was observed, as shown in Fig. 31, demonstrating the useful catalytic properties of PtY particles. This step was necessary as the presence of electrolyte added in the water causes unavoidably facilitated electrolysis. As an example, 0.4 mM NaOH resulted in current densities of the same order of magnitude as those obtained with 10% PtY in pure water (13,53). Besides the solvent, the electrolysis at electrochemically activated microheterogeneous interfaces can be also applied to solutes. This has been observed for a model

* An attractive characteristic of ultramicroelectrodes is their ability to be effectively used in low ionic strength medium (absence of added supporting electrolyte) (211) because the magnitude of both charging and Faradaic currents that flow at a single ultramicroelectrode is very small and can be carried by the few ions in solution.

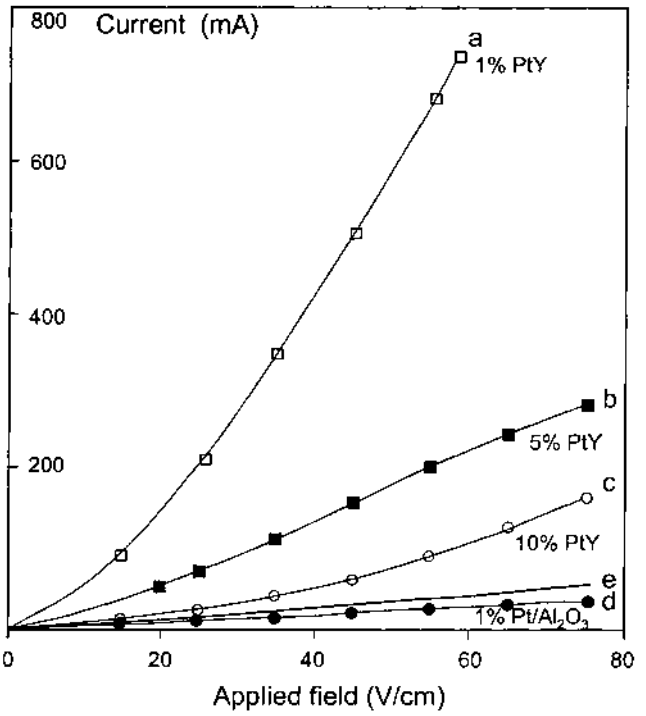

Fig. 31 Current–voltage response for the electrolysis of water by 0.1 g of supported Pt dispersed electrodes. (a) 1% Pt-Y; (b) 5% Pt-Y; (c) 10% Pt-Y; (d) 1% Pt-Al_2O_3; (e) current-potential response at feeder electrodes only for 30 ml of filtrate obtained after stirring suspensions of 0.4 g of 1%, 5%, or 10% Pt-Y/120 ml H_2O. (Reprinted with permission from Ref. 53.)

substrate in aqueous medium: the $Fe(CN)_6^{3-/4-}$ couple using zeolite-supported Pt and RuO_2 catalysts (186). In the presence of electrolyte, the electrolysis time decreased by 55% with dispersed 1% PtY and by 26% with 5% RuO_2Y as compared with electrolysis carried out without dispersed ultramicroelectrode-modified zeolites. In low ionic strength medium both the average Faradaic yields and reaction speed were much higher with 1% PtY or 5% RuO_2Y than those obtained without the catalyst (186).

Electrocatalyzed synthesis or molecular decomposition using microheterogeneous dispersions involves either unmodified zeolites or molecular sieves exchanged with metal species. Potentiostatic oxidative decomposition of toxic chlorinated aromatics and chlorofluorocarbons can be effectively achieved via electrochemically activated dispersions of pure zeolites (184,213–215). The efficiency of the electrocatalytic degradation is function of the zeolite type. For example, decomposition of 1,2-dichlorobenzene in the presence of synthetic faujasites was found to decrease by increasing the Si/Al ratio, underscoring the importance of ion exchange capacity and Lewis acid sites on the process (184). The selective partial oxidation of propene to propylene oxide is possible in low ionic strength aqueous media using dispersions of $(Pd^{II}Cu^{II})$NaY heterogeneous catalysts (182). Selectivity was achieved because of the simultaneous presence of the Pd^{II} and Cu^{II} catalysts and the possibility to work in the absence of added electrolyte. As also mentioned in Sec. V.A of this chapter, the zeolite-associated complex Co(salen)-Y was also exploited as microheterogeneous dispersions to electrocatalyze the reaction of benzyl chloride with CO_2 (185).

E. Potentiometric Detection

Since the pioneering work showing the utility of zeolite membranes for potentiometric sensing of cations (27) and the subsequent demonstration of size selectivity of zeolite A in the detection of sodium ions in the presence of size-excluded tetraethylammonium (TEA) cations (32), other investigations were devoted to potentiometric analysis using zeolite-based membranes. Their analytical characteristics are given in Table 6. Except for the cases of obvious size exclusion, the selectivity observed for non-size-excluded cations remains poor.

Mordenite-type zeolite pellets impregnated with low viscosity epoxy resins were applied to the detection of cesium ions, with a marked preference over other alkali metal cations and some divalent species (99,100). Near-Nernstian potentiometric response was, however, observed because of the rather low zeolite/epoxy adhesion. This can be improved either by choosing an adequate form of zeolite or by optimizing the membrane preparation procedure. Ideal Nernstian response to alkali-metal ions was obtained using copper-exchanged zeolites and membranes lightly loaded with plastic phase (101,102), and NaA-polysulfone coatings on glassy carbon gave rise to extended linear concentration range for detection of cadmium(II) or aluminum(III) in aqueous solution (8). Zeolite-polydimethylsiloxane membranes are not only suited to the potentiometric detection of alkali metal cations; they can also be utilized for surfactant determination by potentiometric titration (103). The use of pressed pure zeolite disks without any added organic binder allows potentiometric detection in nonaqueous media, as exemplified for sodium and TEA in acetonitrile with using zeolite Y (187). A very recent study has demonstrated the possibility of combining an ammonium-selective zeolite (clinoptilolite) with an ion-sensitive field effect transistor (ISFET) device for potentiometric sensing of this species with a remarkable sensitivity down to 10^{-8} M (216). High selectivity was explained by the well-known marked preference of clinoptilolite for ammonium over alkali and alkaline earth metal ions (41).

F. Amperometric Biosensors

A biosensor consists of three components: a biological detection system, a transducer (piezoelectric, acoustic, optical, calorimetric, or electrochemical), and an output system. An amperometric biosensor is an analytical device containing an immobilized biologically sensitive material (enzyme, antibody, antigen, organelles, DNA, cells, tissues, or organic molecules) in contact with or integrated in an electrochemical transducer that ultimately converts a biological signal to a quantitatively measurable electrical signal. One key factor in biosensor construction is the development of immobilization technologies for stabilizing biomolecules and tethering them to surfaces. An important possibility in this construction is the addition of an associated charge-transfer mediator that would increase the detection selectivity by lowering overpotentials (see note 7). This should be mobile enough to act as a cofactor between the biomolecule and the electrode surface and at the same time sufficiently immobilized to ensure long-term stability. Some studies in the amperometric biosensor field were carried out at enzyme-modified zeolite-containing electrodes. Their analytical characteristics are presented in Table 7.

Incorporation of zeolite particles into enzyme-based carbon paste bioelectrodes results in improved sensitivity and extended linear range. These were attributed to higher active enzyme loadings due to the formation of a porous paste network that exposes the enzyme contained in the interior of the paste to the substrate solution, thanks to the hydrophilic character of zeolites (155,166). This effect was further confirmed by using

Table 6 Electroanalytical Applications of Zeolite-Modified Electrodes: Potentiometry

Analyte[a]	Zeolite	Electrode[b]	Medium	Regeneration	Method	Concentration range	Detection limit	Ref.
Al^{3+}	Na-A	Polysulfone membrane	Water		Impregnation	10^{-5}–10^{-1} M		8
Ammonium	Clinoptilolite	Zeolite-silo-prene membrane on ISFET	Water		Impregnation	10^{-7}–10^{-3} M	1×10^{-8} M	216
Alkali-metal ions	Na-, Cu-, Fe-A, Na-, Cu-, Fe-X	Resin-impregnated membrane	Water	Equilibration in water	Impregnation	1×10^{-4}–1 M	1–6×10^{-5} M	101, 102
Alkali-metal ions	Na-A, Na-X, Na-Y	Zeolite-PDMS membrane	Water		Impregnation	2×10^{-4}–10^{-1} M	3–7×10^{-5} M	103
Cd^{2+}	Na-A	Polysulfone membrane	Water		Impregnation	10^{-5}–10^{-2} M		8
Cs^{+}	Na-mordenite, Na-A	Resin-impregnated membrane	Water	Equilibration in 0.1 M CsCl	Impregnation	3×10^{-5}–1×10^{-1} M	2×10^{-5} M	99, 100
Na^{+}, TEA^{+}	Na-Y	Pressed zeolite disk	Water, acetonitrile		Impregnation	5×10^{-4}–9×10^{-3} M		187

[a]Abbreviation: TEA^{+}, tetraethylammonium.
[b]Abbreviations: ISFET, ion-sensitive field effect transistor; PDMS, polydimethylsiloxane.

Table 7 Electroanalytical Applications of Zeolite-Modified Electrodes: Biosensors

Analyte	Zeolite	Electrode[a]	Medium	Regeneration	Method[b]	Concentration range	Detection limit	Ref.
Catechol	Various dealuminated H-Y	Zeolite-modified CP + tyrosinase	Phosphate buffer (pH 6)	Mechanical	A (reduction) FIA	2×10^{-5}–1×10^{-4} M		158
Glucose	Na-Y	Zeolite-modified CP + glucose oxidase	Phosphate buffer (pH 7.2)	Mechanical	A (reduction)	1×10^{-4}–2×10^{-3} M		155
Glucose	Dealuminated Y	Zeolite + immobilized glucose oxidase + PVA, coated on platinum	Phosphate buffer (pH 7.0)		A (oxidation)	2×10^{-6}–3×10^{-3} M	0.5 μM	75
Glucose	Zeolite beta	Zeolite + immobilized glucose oxidase + TCNQ, dispersed in CP	Phosphate buffer (pH 7)		CV, A (oxidation)	5×10^{-6}–2×10^{-3} M		166
Glucose	Na-Y/ruthenium purple	Zeolite + glucose oxidase + GluA + BSA, coated on SnO_2	Phosphate buffer (pH 5.1)		LSV, A (FIA) (reduction)	10^{-6}–10^{-3} M	0.1 μM	81
H_2O_2	Na-Y/methylene green	Zeolite + PS coating on GC, + immobilized POD	Phosphate buffer (pH 6.5)		A (reduction)	5×10^{-6}–7.5×10^{-4} M		82
Phenol, *p*-cresol, 4-chlorophenol	Various dealuminated H-Y	Zeolite-modified CP + tyrosinase	Phosphate buffer (pH 6)	Mechanical	A (reduction) FIA	2×10^{-5}–1×10^{-4} M		158
Phenol	Na-Y	Zeolite-modified screen printed carbon ink + tyrosinase + NMP^+	Phosphate buffer (pH 6.8)		A (reduction)	0.25 nM–60 μM	0.25 nM	177

[a] Abbreviations: CP, carbon paste; PVA, poly(vinyl alcohol); TCNQ, tetracyanoquinidimethane; GluA, glutaraldehide; BSA, bovine serum albumin; GC, glassy carbon; POD, horseradish peroxidase; NMP^+, 5-methylphenazonium.

[b] Abbreviations: A, amperometry; FIA, flow injection analysis; CV, cyclic voltammetry; LSV, linear scan voltammetry.

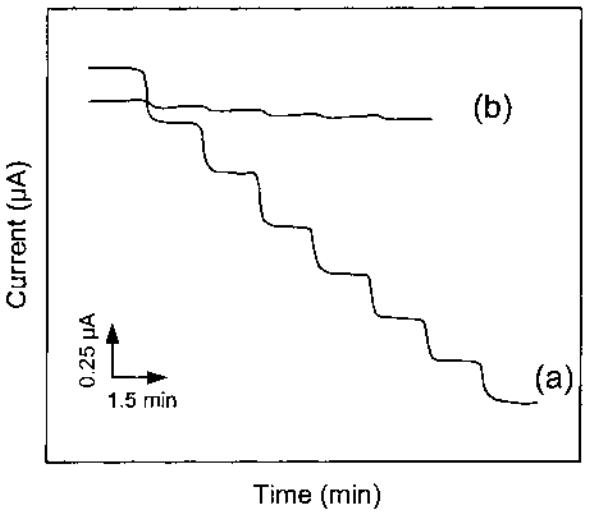

Fig. 32 Current output for catalytic oxidation of glucose with delaluminated zeolite Y/glucose oxidase–modified platinum electrode (a) and NaY/glucose oxidase–modified platinum electrode (b). Successive additions of 0.1 mM glucose; operating potential, +0.55 V. (Reprinted with permission from Ref. 75.)

several HY zeolite powders in a tyrosinase-based carbon paste electrode, dealuminated to various extents, showing higher improvement the more hydrophilic the zeolite. The most hydrophobic Y samples did not result in any enhancement in the electrode response in comparison with the tyrosinase electrode without added zeolite (158). Due to the rather narrow-channel network of zeolites relative to the size of the enzymes, these porous solids are apparently not attractive candidates to immobilize the biomolecules by physical entrapment, i.e., contrary to sol-gel silicates (217). In any event, it was shown that dealuminated zeolite Y (obtained by hydrothermal treatment and subsequent calcination of NH_4Y) displays an adequate surface charge and an open structure large enough to accommodate glucose oxidase (75). When coated on a platinum electrode surface, the resulting biosensor gives rise to well-defined amperometric response to glucose—better by far than that obtained with glucose oxidase simply adsorbed onto the surface of untreated zeolite Y, as can be noted in Fig. 32.

Another use of zeolites in the biosensing field exploits their ability to concentrate positively charged mediators by ion exchange. Several examples are available in the ZME literature (81,82,166,177). The mediation process often proceeds well, but long-term stability of the biosensor suffers from leaching of the cationic mediator into the external solution as a consequence of back ion exchange with the supporting electrolyte cations (12,82).

G. Batteries and Fuel Cells

The marked interest in using zeolite molecular sieves in the fabrication of power sources is pointed out by the numerous patents that have been registered in this field. Zeolites were either used alone or associated with organic polymers as solid electrolytes in batteries (34,132,134,135,137,140,142). This kind of application arises from the facts that zeolites are fairly good solid-state ionic conductors with relatively small activation energies for

conduction and are stable over a wide temperature range. In early 1965, in a pioneering study, Freeman had already proposed a design of zeolite batteries operating well at both low and high temperatures (−78°C and 500°C) (33). The cell composition was made of a multilayer arrangement of a gold cathode contact, a copper-exchanged zeolite X catholyte, a sodium zeolite X separator, and a zinc anode (Au|Cu^{II}X|NaX|Zn). Operational working of the cell involves Zn oxidation and Cu^{II} reduction accompanied by charge compensation via the NaX separator (migration of Na^+ toward the cathodic part of the cell). Following Freeman's idea, zeolite-based microporous solid electrolytes were used in the fabrication of lithium secondary batteries, with the zeolite acting as a host for lithium ions (134,137,138, 140–142,218). Zeolite was also host for Zn^{II} in zinc-manganese oxide batteries (136), for Pb^{II} in lead-acid batteries (133), or for Na^+ to prepare sodium anodes (55). When zeolite-polymer composites are used as solid electrolytes, the zeolite component is often exploited to increase ionic conductivity, which is especially useful for operation of batteries at low temperature (132,137,139). Titanosilicalites are also interesting in this respect (219,220). The desiccant properties of zeolites were exploited in manufacturing batteries to remove trace water from nonaqueous electrolytes after assembly of the cell (134,217,221–226), which contributes to lowering the self-discharge rate of the battery. In sealed lead-acid batteries, the addition of zeolite enhances the absorption of oxygen and suppresses the evolution of hydrogen (227,228). It also acts as an oxygen concentrator in zinc-oxygen batteries (229) or as a gas-adsorbing material between the anodic and cathodic parts of the cell (230). Zeolite modification of organic cathodes was proposed as a clean technology for improved cycle life of the zinc-chloranil organic secondary battery (231). In addition, one should mention the use of dehydrated zeolite crystals as host structures for liquid and/or volatile electrochemically active species in designing solid-state batteries: examples are available for zeolite/iodine and zeolite/sulfur (or selenium) cathodes, which can be readily applied at room temperature (54,55,132).

Ionically conductive zeolites are attractive materials in the fabrication of fuel cell electrodes. They often serve as a support for catalytic metals such as Ag and Pd (35), or other noble metals such as Rh, Pt, Ru, and Ni (232,233). Zeolites were also added in the membrane of hydrogen-oxygen fuel cells for their water-absorptive capacity (36). The intrinsic catalytic properties of zeolites NaA and NaX were exploited in oxygen-methanol fuel cells with efficiencies comparable to those of noble metal cathodes (234,235). Silver-exchanged zeolite A was found to electrocatalyze oxygen reduction in such fuel cells (236). Zeolite membranes separating the anode and cathode compartments allow the passage of ions through the membrane to carry an electric current in methanol fuel cells using a basic electrolyte such as carbonate: the zeolite membrane prevents the escape of methanol into the atmosphere, which enables the fuel cell to operate at higher temperature and hence to be more efficient (237). Acidic zeolite matrices for fuel cells were also reported (238).

H. Photoelectrochemistry

Zeolites are excellent templates for the fabrication of multicomponent electron transfer systems, but most often these are photochemically induced (see Chapter 13 in this volume), with the sacrificial electron feeder or consumer being a chemical oxidant or reducer and not an electrode surface (180). It is somewhat surprising that photoelectrochemistry involving zeolite molecular sieves has been so sparingly considered.

The photocatalytic oxidation of water to molecular oxygen can be achieved on thin AgCl-coated electrodes, with the metallic silver produced during the process being

electrochemically reoxidized (239). Because of the attractive features of silver chloride–containing zeolites, the above system can be advantageously replaced by a zeolite AgA–modified electrode immersed in a chloride solution (72). A combined photochemical and electrochemical study of silver(zero)–Y zeolite exchanged with methyl viologen was reported, which was applied to photoreduction of intrazeolitic methyl viologen by silver clusters stabilized in or on zeolite Y (80). A recent investigation of $Ru(bpy)_3^{2+}/TiO_2$-codoped zeolites was conducted to demonstrate electron transfer photocatalysis (173). It was found that the TiO_2 nanoparticles located in close vicinity to the zeolite particles have the role of electron relay to reach electroactive species entrapped in the zeolite structure.

I. Electrochemical Characterization of Reactions in Zeolites

Electrochemistry at ZMEs can be useful for characterizing the physicochemical processes taking place in zeolites and for probing reactions occurring in the presence of zeolite particles. Three illustrative recent examples are described below.

The normalized ion-exchange isotherm corresponding to methyl viologen–sodium exchange in zeolite Y can be constructed rapidly from voltammetric data recorded at a zeolite Y–modified carbon paste electrode (169). The method is based on measurement of the equivalent fraction of methyl viologen in the zeolite after equilibration in a solution containing a selected equivalent fraction of solution phase methyl viologen (selected MV^{2+}/Na^+ ratio). Only the zeolite particles located at the electrode surface (few micrograms) are in contact with the external solution (typically 50 ml), which implies a very low solid-to-solution ratio. As a consequence, the macroscopic composition of the solution remains unchanged during the equilibration process. The equivalent fractions in solution are thus known, and plotting them against the electrochemically measured equivalent fractions in zeolite gives the corresponding normalized ion-exchange isotherm. This method is much faster by far than the classical approach based on batch analyses.

Chronoamperometry applied to ZME containing partially silver ion-exchanged faujasites can be applied to determine accurately intrazeolite diffusion coefficients (78). The approach is based on the fact that reduction of silver(I) at the electrode surface requires its preceding leaching out of the zeolite framework. In case of silver(I) located in the small cages, the rate-determining step is the intrazeolite diffusion from the small-channel system to the large supercages. From simulation of the chronoamperometric curves according to a CE mechanism, with "C" for chemical (diffusion) and "E" for electrochemical (electron transfer), it is possible to calculate the intrazeolite diffusion coefficient, as $2–4 \times 10^{-8}$ cm^2/s for Ag^+ in Y.

The third example is illustrated in Fig. 33 and concerns the electrochemical evidence of impeded attack of water at thianthrene radical cation ($TH^{\bullet+}$) when it is stabilized on the outermost layers of zeolites; similar impeded attacks were also observed for the radical anion ($TH^{\bullet-}$) and for radical ions of anthracene ($AN^{\bullet+/\bullet-}$) (84). On unmodified carbon paste electrodes, solution phase TH is electrochemically oxidized into $TH^{\bullet+}$ at about $+1.18$ V vs. SCE. In the absence of water, $TH^{\bullet+}$ is subsequently oxidized (into transient TH^{2-}) at $+1.68$ V (curve a of Fig. 33), whereas the presence of trace water results in the formation of thianthrene oxide, oxidation of which is more difficult, leading to the almost complete replacement of the peak at $+1.68$ V by a peak at $+1.82$ V (curve b of Fig. 33). In contrast, when TH is trapped on the external surface of mordenite the voltammetric curve recorded at the zeolite modified carbon paste electrode in the presence of 2% water reflects the existence of a well-defined signal at $+1.65$ V (in addition to the $TH \rightarrow TH^{\bullet+}$ process at $+1.18$ V), indicating that $TH^{\bullet+} \rightarrow TH^{2+}$ oxidation is still the predominant process

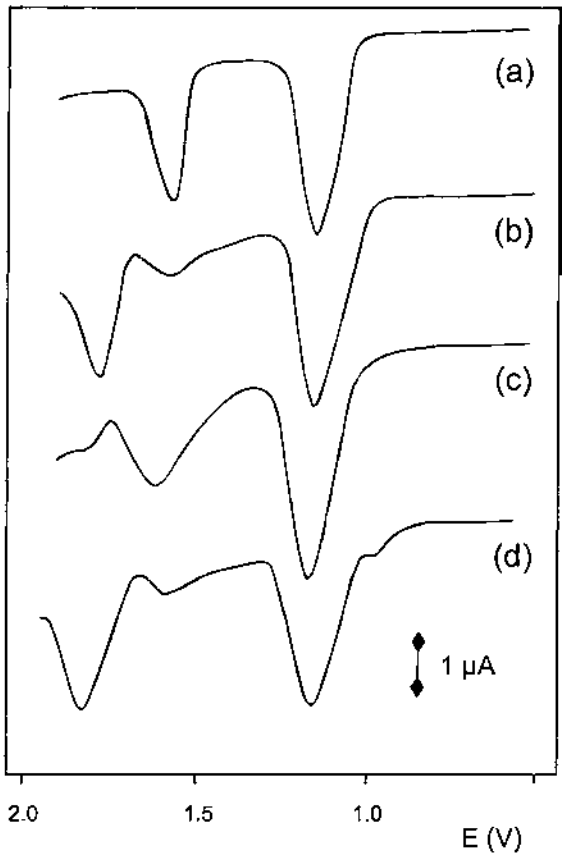

Fig. 33 Differential pulse voltammetry of thrianthrene solution (1.0 nM) in acetonitrile using Et_4NClO_4 (0.10 M): (a) in the presence of alumina; (b) same as (a) but in the absence of alumina using routinely dried acetonitrile containing minor amounts of residual water; (c) Polymer-coated film zeolite–modified electrode containing thianthrene adsorbed in mordenite immersed in a acetonitrile/water (98:2) solution having Et_4NClO_4 (0.10 M) as electrolyte; (d) solid thianthrene (no zeolite) deposited on the glassy carbon electrode under conditions identical to those in (c). The potential scan rate was 20 mV/s and the pulse width 10 mV. (Reprinted with permission from Ref. 84.)

(curve c in Fig. 33). This demonstrates that $TH^{\bullet+}$ on the zeolite surface is effectively protected against the attack of water. A control experiment with solid TH on the electrode without zeolite was conducted to provide further evidence of the stabilizing role of the zeolite, demonstrating a similar behavior as for solution phase TH (comparison of curves b and d in Fig. 33). This illustrates the usefulness of electrochemistry at ZMEs to gather information about the particular reactivity of electroactive guest molecules located on the zeolite boundaries.

ACKNOWLEDGMENTS

I thank those colleagues who have significantly contributed to outstanding works in the fields of electrochemistry involving zeolite molecular sieves. Special acknowledgment is

also due to several publishing houses for giving permission to reproduce copyrighted artwork materials that have appeared in their journals.

REFERENCES

1. RW Murray. Acc Chem Res 13:135–141, 1980.
2. RW Murray, AG Ewing, RA Durst. Anal Chem 59:379A–390A, 1987.
3. RW Murray. In: AJ Bard, ed. Electroanalytical Chemistry, Vol 13. New York: Marcel Dekker, 1984, pp 191–368.
4. RW Murray. Proc Robert A Welch Found Conf Chem Res 30:168–218, 1986.
5. JS Miller, ed. Chemically Modified Surfaces in Catalysis and Electrocatalysis. ACS Symp Ser No. 192. Washington, DC: American Chemical Society, 1988.
6. RW Murray. In: RW Murray, ed. Molecular Design of Electrode Surfaces (Techniques of Chemistry, Vol 22). New York: Wiley, 1992, pp 1–48.
7. DR Rolison. Chem Rev 90:867–878, 1990.
8. DR Rolison, RJ Nowak, T Welsh, CG Murray. Talanta 38:27–35, 1991.
9. DR Rolison. Stud Surf Sci Catal 85:543–586, 1994.
10. A Walcarius. Electroanalysis 8:971–986, 1996.
11. L Roué, E Briot, F Bedioui. Can J Chem 76:1886–1909, 1998.
12. A Walcarius. Anal Chim Acta 384:1–16, 1999.
13. DR Rolison, CA Bessel. Acc Chem Res 33:737–744, 2000.
14. GA Ozin, A Kuperman, A Stein. Angew Chem Int Ed Engl 28:359–376, 1989.
15. D Rong, H-G Hong, Y Kim, JS Krueger, JE Mayer, TE Mallouk. Coord Chem Rev 97:237–248, 1990.
16. AJ Bard, TE Mallouk. In: RW Murray, ed. Molecular Design of Electrode Surfaces. New York: Wiley, 1992, pp 271–312.
17. MD Baker, C Senaratne. In: J Lipkowski, PN Ross, eds. The Electrochemistry of Novel Materials. New York: VCH, 1994, pp 339–380.
18. F Bedioui. Coord Chem Rev 144:39–68, 1995.
19. PK Dutta, M Ledney. Progr Inorg Chem 44:209–271, 1997.
20. E Briot, F Bedioui. Curr Topics Electrochem 4:87–99, 1997.
21. A Walcarius. Recent Res Devel Electrochem 1:265–280, 1998.
22. MD Baker, C Senaratne, M McBrien. J Phys Chem 99:12367, 1995.
23. J Li, K Pfanner, G Calzaferri. J Phys Chem 99:12368–12369, 1995.
24. C Senaratne, J Zhang, MD Baker, CA Bessel, DR Rolison. J Phys Chem 100:5849–5862, 1996.
25. F Bedioui, J Devynck, KJ Balkus Jr. J Phys Chem 100:8607–8609, 1996.
26. DR Rolison, CA Bessel, MD Baker, C Senaratne, J Zhang. J Phys Chem 100:8610–8611, 1996.
27. CE Marshall. J Phys Chem 43:1155–1164, 1939.
28. CE Marshall, WE Bergman. J Am Chem Soc 63:1911–1916, 1941.
29. CE Marshall, CA Krinbill. J Am Chem Soc 64:1814–1819, 1942.
30. CE Marshall, AD Ayer. J Am Chem Soc 70:1297–1302, 1948.
31. CE Marshall. J Phys Chem 52:1284–1295, 1948.
32. RM Barrer, SD James. J Phys Chem 64:417–427, 1960.
33. DC Freeman. US Patent Number 3,186,875 (1965), Br Patent No. 999,948 (1965).
34. CC Liang. Ger Patent No. 2,228,843 (1973).
35. AM Moos. US Patent No. 3,097,115 (1963), Ger Patent Number 1,302,003 (1969).
36. C Berger, PM Strier. Adv Chem Ser 64:17–29, 1967.
37. MV Susic, N Petranovic. Some forms of synthetic zeolites as solid electrolytes. Extended abstracts of the 28th Meeting of the International Society of Electrochemistry, Druzhba, 1977; RV Moshtev, ed.; ISE: Sofia, Bulgaria, pp 534–536.

38. MV Susic, N Petranovic. Electrochim Acta 23:1271–1274, 1978.
39. MV Susic. Electrochim Acta 24:535–540, 1979.
40. N Petranovic, MV Susic. Zeolites 3:271–273, 1983.
41. DW Breck. Zeolite Molecular Sieve. Structure, Chemistry, and Use, 2nd ed. Malabar: Krieger, 1984, pp 529–592.
42. R Messina, JP Pereira-Ramos, D Barboux, F Petit, J Perichon, JF Fauvarque. Fr Patent No. 81,21,313 (1981).
43. J-P Pereira-Ramos, R Messina, J Perichon. J Electroanal Chem 146:157–169, 1983.
44. CG Murray, RJ Nowak, DR Rolison. J Electroanal Chem 164:205–210, 1984.
45. B de Vismes, F Bedioui, J Devynck, C Bied-Charreton. J Electroanal Chem 187:197–202, 1985.
46. P Hernandez, E Alda, L. Hernandez. Fresenius J Anal Chem 327:676–678, 1987.
47. HA Gemborys, BR Shaw. J Electroanal Chem 208:95–107, 1986.
48. BR Shaw, KE Creasy, CJ Lanczycki. JA Sargeant, M Tirhado. J Electrochem Soc 135:869–876, 1988.
49. S Mintova, V Valtchev, V Engström, BJ Schoeman, J Sterte. Micropor Mater 11:149–160, 1997.
50. V Engström, B Mihailova, J Hedlund, A Holmgren, J Sterte. Micropor Mater 38:51–60, 2000.
51. Y Kiyozumi, F Mizukami, K Maeda, M Toba, S-I Niwa. Adv Mater 8:517–520, 1996.
52. DR Rolison, RJ Nowak, S Pons, J Ghoroghchian, M Fleischmann. In: FL Carter, RE Siatkowski, H Wohltjen, eds. Molecular Electronic Devices. North-Holland: Elsevier, 1988, pp 401–410.
53. DR Rolison, EA Hayes, WE Rudzinski. J Phys Chem 93:5524–5531, 1989.
54. J Coetzer. Electrochim Acta 23:787–789, 1978.
55. J Coetzer. Ger Patent Number 2,810,320 (1978), Ger Patent No. 2,928,863 (1980), Ger Patent Number 2,935,686 (1980), Ger Patent Number 2,942,764 (1980), Fr Patent No. 2,492,173 (1982).
56. Z Li, TE Mallouk. J Phys Chem 91:643–648, 1987.
57. Z Li, CM Wang, L Persaud, TE Mallouk. J Phys Chem 92:2592–2597, 1988.
58. C Iwakura, S Miyazaki, U Yoneyama. J Electroanal Chem 246:63–72, 1988.
59. J Cassidy, E O'Donoghue, W Breen. Analyst 114:1509–1510, 1989.
60. J Cassidy, W Breen, E O'Donoghue, MEG Lyons. Electrochim Acta 36:383–384, 1991.
61. KLN Phani, S Pitchumani. Electrochim Acta 37:2411–2414, 1992.
62. S Bharathi, KLN Phani, J Joseph, S Pitchumani, D Jeyakumar, GP Rao, SK Rangarajan. J Electroanal Chem 334:145–153, 1992.
63. C Senaratne, MD Baker. J Electroanal Chem 332:357–364, 1992.
64. MD Baker, C Senaratne, J Zhang. J Chem Soc Faraday Trans 88:3187–3192, 1992.
65. J Li, G Calzaferri. J Chem Soc Chem Commun 1993:1430–1432.
66. MD Baker, C Senaratne, J Zhang. J Phys Chem 98:1668–1673, 1994.
67. C Senaratne, MD Baker. J Phys Chem 98:13687–13694, 1994.
68. J Li, G Calzaferri. J Electroanal Chem 377:163–175, 1994.
69. MD Baker, J Zhang, M McBrien. J Phys Chem 99:6635–6639, 1995.
70. J Li, K Pfanner, G Calzaferri. J Phys Chem 99:2119–2126, 1995.
71. G Calzaferri, M Lanz, J Li. J Chem Soc Chem Commun 1995:1313–1314.
72. G Calzaferri, N Gfeller, K Pfanner. J Photochem Photobiol A Chem 87:81–84, 1995.
73. A Walcarius, T Barbaise, J Bessière. Anal Chim Acta 340:61–76, 1997.
74. P Lainé, R Seifert, R Giovanoli, G Calzaferri. New J Chem 21:453–460, 1997.
75. B Liu, R Hu, J Deng. Anal Chem 69:2343–2248, 1997.
76. DH Brouwer, MD Baker. J Phys Chem B 101:10390–10397, 1997.
77. L Mogensen, L Kryger, Electroanalysis 10:1285–1287, 1998.
78. MD Baker, M McBrien, I Burgess, J Phys Chem B 102:2905–2907, 1998.
79. V Ganesan, R Ramaraj. Langmuir 14:2497–2501, 1998.
80. WS Szulbinski. Inorg Chim Acta 269:253–259, 1998.

81. CF Chen, CM Wang. J Electroanal Chem 466:82–89, 1999.
82. B Liu, F Yan, J Kong, J Deng. Anal Chim Acta 386:31–39, 1999.
83. MD Baker, C Senaratne. Phys Chem Chem Phys 1:1673–1677, 1999.
84. A Doménech, I Casades, H Garcia. J Org Chem 64:3731–3735, 1999.
85. A Doménech, MT Doménech-Carbo, H Garcia, MS Galletero. Chem Commun 1999:2173–2174.
86. MD Baker, TW Hui. Electrochemistry of methyl viologen-exchanged zeolite Y modified electrodes. Proceedings of the 12th International Zeolite Conference, Baltimore, 1999; MMJ Treacy, ed.; Materials Research Society, Warrendale, PA, pp 2073–2078.
87. A Doménech, P Formentin, H Garcia, MJ Sabater. Eur J Inorg Chem 2000:1339–1344.
88. A Doménech, A Corma, H Garcia, S Valencia. Topics Catal 11/12:401–407, 2000.
89. TW Hui, MD Baker. J Phys Chem B 105:3204–3210, 2001.
90. G Calzaferri, K Hädener, J Li. J Chem Soc Chem Commun 1991:653–654.
91. JB Talbot, CB Ahlers. Electrophoretic deposition of zeolites. Abstract of the 217th ACS National Meeting, Anaheim, 1999, pp 21–25.
92. CB Ahlers, JB Talbot. J Electrochem Soc 146:3259–3263, 1999.
93. CB Ahlers, JB Talbot. Electrochim Acta 45:3379–3387, 2000.
94. MD Baker, C Senaratne. Anal Chem 64:697–700, 1992.
95. V Ganesan, R Ramaraj. J Appl Electrochem 30:757–760, 2000.
96. KLN Phani, S Pitchumani, SK Ravichandran. Langmuir 9:2455–2459, 1993.
97. Y-X Jiang, W-B Song, Y Liu, N Lü, M-Z Zou, H-D Xu, A-L Zhang. Chem J Chinese Univ 20:717–721, 1999.
98. SK Ravichandran, KLN Phani, S Pitchumani. Zeolite-conducting polyaniline hybrid: synthesis and its electrochemical behavior. Proceedings of the IUPAC International Symposium on Advanced Polymer Science and Technology. KSV Srinivasan, ed.; Allied Publishers, Ltd., New Delhi, India, 1:347–350, 1998.
99. G Johansson, L Risinger, L Fälth. Anal Chim Acta 119:25–32, 1980.
100. G Johansson, L Fälth, L Risinger. Hung Sci Instr 49:47–51, 1980.
101. M Demertzis, NP Evmiridis. J Chem Soc Faraday Trans I 82:3647–3655, 1986.
102. NP Evmiridis, MA Demertzis, AG Vlessidis. Fresenius J Anal Chem 340:145–152, 1991.
103. S Matysik, F-M Matysik, J Mattusch, W-D Einicke. Electroanalysis 10:98–102, 1998.
104. MD Baker, J Zhang. J Phys Chem 94:8703–8708, 1990.
105. Y Jiang, M Zou, K Yuan, H Xu. Electroanalysis 11:254–259, 1999.
106. K Lee, C Lee, JW Park, YS Park, KB Yoon. Bull Korean Chem Soc 20:1365–1367, 1999.
107. N Venkatathri, MP Vinod, K Vijayamohanan, S Sivasanker. J Chem Soc Faraday Trans 92:473–478, 1996.
108. MP Vinod, TK Das, AJ Chandwadkar, K Vijayamohanan, JG Chandwadkar. Mater Chem Phys 58:37–43, 1999.
109. CA Bessel, DR Rolison. J Phys Chem B 101:1148–1157, 1997.
110. KE Creasy, YP Deng, J Park, EVR Borgstedt, SP Davis, SL Suib, BR Shaw. Mater Res Soc Symp Proc 233:157–167, 1991.
111. RAW Dryfe, SM Holmes. J Electroanal Chem 483:144–149, 2000.
112. F Bedioui, E de Boysson, J Devynck, KJ Balkus Jr. J Electroanal Chem 315:313–318, 1991.
113. F Bedioui, E de Boysson, J Devynck, KJ Balkus Jr. J Chem Soc Faraday Trans 87:3831–3834, 1991.
114. K Mesfar, B Carré, F Bedioui, J Devynck. J Mater Chem 3:873–876, 1993.
115. L Gaillon, N Sajot, F Bedioui, J Devynck, KJ Balkus Jr. J Electroanal Chem 345:157–167, 1993.
116. F Bedioui, L Roué, L Gaillon, J Devynck, SL Bell, KJ Balkus Jr. Prepr Am Chem Soc Div Pet Chem 38:529–535, 1993.
117. F Bedioui, L Roué, E Briot, J Devynck, SL Bell, KJ Balkus Jr. J Electroanal Chem 373:19–29, 1994.
118. AG Gabrielov, KJ Balkus Jr, SL Bell, F Bedioui, J Devynck. Micropor Mater 2:119–126, 1994.

119. F Bedioui, L Roué, J Devynck, KJ Balkus Jr. J Electrochem Soc 141:3049–3052, 1994.
120. L Gaillon, F Bedioui, J Devynck. J Mater Chem 4:1215–1218, 1994.
121. F Bedioui, L Roué, J Devynck, KJ Balkus Jr. Stud Surf Sci Catal 84:917–924, 1994.
122. KJ Balkus Jr, AG Gabrielov, S Bell, F Bedioui, L Roué, J Devynck. Inorg Chem 33:67–72, 1994.
123. F Bedioui, L Roué, E Briot, J Devynck, KJ Balkus Jr, JF Diaz. New J Chem 20:1235–1241, 1996.
124. KJ Balkus Jr, AK Khanmamedova, KM Dixon, F Bedioui. Appl Catal A 143:159–173, 1996.
125. F Bedioui, E Briot, J Devynck, KJ Balkus Jr. Mater Res Soc Symp Proc 431:45–50, 1996.
126. F Bedioui, E Briot, J Devynck, KJ Balkus Jr. Inorg Chim Acta 254:151–155, 1997.
127. E Briot, F Bedioui, KJ Balkus Jr. J Electroanal Chem 454:83–89, 1998.
128. MANDA Lemos, P Sousa, F Lemos, AJL Pombeiro, FR Ribeiro. Stud Surf Sci Catal 122:443–446, 1999.
129. BR Shaw, KE Creasy. Electrochemistry in dry zeolite crystals. Abstract of the 8th International Zeolite Conference, Amsterdam, 1989.
130. KE Creasy, BR Shaw. J Electrochem Soc 137:2353–2354, 1990.
131. N Petranovic, D Minic. Ceram Int 22:317–320, 1996.
132. MM Thackeray, J Coetzer. Solid State Ionics 6:135-138, 1982; J Coetzer, MJ Nolte, A Steynberg. Fr Patent No. 2,463,982 (1981).
133. Furukawa Battery Co., Ltd. Jp Patent No. 58,012,263 (1983).
134. Sanyo Electric Co., Ltd. Jp Patent No. 58,103,776 (1983).
135. D Wang, W Yu, B Zhu, W Yuan, X Jia. Chn Patent No. 86,103,796 (1987).
136. W Yang, H Yang, J Zhang. Dianchi 21:3–5, 1991.
137. S Slane, M Salomon. J Power Sources 55:7–10, 1995.
138. Y Fang. Yingyong Huaxue 12:24–28, 1995.
139. N Munichandraiah, LG Scanlon, RA Marsh, B Kumar, AK Sircar. J Appl Electrochem 25:857–863, 1995.
140. T Inemasu, H Yoshihisa. Jp Patent No. 10,270,018 (1998).
141. F Gao, PH Mitchell, J Barker, J Swoyer. US Patent No. 5,728,489 (1998).
142. DH Jang, SH Kim, HJ Kim, SM Hong. World Patent No. 2000,038,263 (2000).
143. O Enéa. Electrochim Acta 34:1647–1651, 1989.
144. RN Adams. Electrochemistry at Solid Elecrodes. New York: Marcel Dekker, 1969.
145. K Kalcher, J-M Kauffmann, J Wang, I Svancara, K Vytras, C Neuhold, Z Yang. Electroanalysis 7:5–22, 1995.
146. J Wang, T Martinez. Anal Chim Acta 207:95–102, 1988.
147. KE Creasy, BR Shaw. Electrochim Acta 33:551–556, 1988.
148. N El Murr, M Kerkeni, A Sellami, Y Bentaarit. J Electroanal Chem 246:461–465, 1988.
149. S de Castro-Martins, S Khouzami, A Tuel, Y Bentaarit, N El Murr, A Sellami. J Electroanal Chem 350:15–28, 1993.
150. A Walcarius, L Lamberts, EG Derouane. Electrochim Acta 38:2257–2266, 1993.
151. A Walcarius, L Lamberts, EG Derouane. Electrochim Acta 38:2267–2276, 1993.
152. M Xu, W Horsthemke, M Schell. Electrochim Acta 38:919–925, 1993.
153. S de Castro-Martins, A Tuel, Y Bentaarit. Zeolites 14:130–136, 1994.
154. A Walcarius, L Lamberts, EG Derouane. Electroanalysis 7:120–128, 1995.
155. J Wang, A Walcarius. J Electroanal Chem 404:237–242, 1996.
156. J Wang, A Walcarius. J Electroanal Chem 407:183–187, 1996.
157. C Bing, L Kryger. Talanta 43:153–160, 1996.
158. G Marko-Varga, E Burestedt, CJ Svensson, J Emnéus, L Gorton, T Ruzgas, M Lutz, KK Unger. Electroanalysis 8:1121–1126, 1996.
159. A Walcarius, L Lamberts. J Electroanal Chem 422:77–89, 1997.
160. B Chen, N-K Goh, L-S Chia. Electrochim Acta 42:595–604, 1997.
161. MZ Zou, HD Xu, J Lu, QH Ru. Chinese Chem Lett 8:247–250, 1997.

162. IN Rodriguez, JA Munoz-Leyva, JL Hidalgo-Hidalgo de Cisneros. Anal Chim Acta 344:167–173, 1997.
163. A Walcarius, T Barbaise, J Bessière. Ion exchange voltammetry at zeolite modified electrodes versus ion exchange in zeolites. Proceedings of the Joint 142th Meeting of the Electrochemical Society and 48th Meeting of the International Society of Electrochemistry, Paris, 1997, Vol 97-19; AJ Ricco, MA Butler, P Vanysek, G Horval, AF Silva, eds,; ECS: Pennington, NJ, pp 504–513.
164. A Walcarius, L Lamberts. Anal Lett 31:585–599, 1998.
165. SV Guerra, CR Xavier, S Nakagaki, LT Kubota. Electroanalysis 10:462–466, 1998.
166. B-H Liu, R-Q Hu, H-Y Liu, J-Q Deng. Acta Chim Sinica 56:682–687, 1998.
167. A Walcarius. Anal Chim Acta 388:79–91, 1999.
168. A Walcarius, V Vromman, J Bessière. Sensors Actuators B 56:136–143, 1999.
169. A Walcarius, P Mariaulle, L Lamberts. J Electroanal Chem 463:100–108, 1999.
170. A Walcarius, S Rozanska, J Bessière, J Wang. Analyst 124:1185–1190, 1999.
171. A Walcarius, P Mariaulle, C Louis, L Lamberts. Electroanalysis 11:393–400, 1999.
172. M Cordero-Rando, M Barea-Zamora, JM Barbera-Salvador, IN Rodriguez, JA Munoz-Leyva, JL Hidalgo-Hidalgo de Cisneros. Mikrochim Acta 132:7–11, 1999.
173. SH Bossmann, C Turro, C Schnabel, MR Pokhrel, LM Payawan Jr, B Baumeister, M Wörner. J Phys Chem B 105:5374–5382, 2001.
174. BR Shaw, KE Creasy. Anal Chem 60:1241–1244, 1988.
175. BR Shaw, KE Creasy. J Electroanal Chem 243:209–217, 1988.
176. BR. Shaw, KE Creasy. US Patent No. 4,957,593 (1990).
177. H Kotte, B Gründig, K-D Vorlop, B Strehlitz, U Stottmeister. Anal Chem 67:65–70, 1995.
178. Z Li, C Lai, TE Mallouk. Inorg Chem 28:178–182, 1989.
179. J Sarradin, J-M Louvet, R Messina, J Perichon. Zeolites 4:157–162, 1984.
180. JS Krueger, TE Mallouk. In: M Gratzel, K Kalyanasundaram, eds. Kinetics and Catalysis in Microheterogeneous Systems. Surf Sci Ser 38:461–490, 1991.
181. DR Rolison, JZ Stemple, DJ Curran. Electrochemical and electric-field effects at dispersions of zeolites. Proceedings of the 9th International Zeolite Conference, Montreal, 1992, pp 699–708.
182. DR Rolison, JZ Stemple. J Chem Soc Chem Commun 1993:25–27.
183. DN Blauch, DR Rolison. J Electroanal Chem 370:305–308, 1994.
184. EA Hayes, JZ Stemple, DR Rolison. In: TL Rose, OJ Murphy, eds. Water Purification by Photoelectrochemical, Photochemical, and Electrochemical Processes. Pennington: Electrochemical Society, 1994, pp 121–130.
185. CA Bessel, DR Rolison. J Am Chem Soc 119:12673–12674, 1997.
186. CA Bessel, DR Rolison. J Electroanal Chem 439:97–105, 1997.
187. RAW Dryfe, P Hayes, SM Holmes. Analyst 126:733–735, 2001.
188. AJ Bard, LR Faulkner. Electrochemical Methods: Fundamentals and Applications. New York: Wiley, 1980.
189. KB Yoon. Chem Rev 93:321–339, 1993.
190. Y Kim, K Seff. J Phys Chem 82:1071–1077, 1978.
191. MD Baker, M McBrien, C Liu, DH Brouwer. Silver nucleation and growth at zeolite modified electrodes. Proceedings of the 12th International Zeolite Conference, Baltimore, 1999, pp 2137–2142.
192. T Sun, K Seff. Chem Rev 94:857–870, 1994.
193. C Senaratne, J. Zhang, J Fox, I Burgess, MD Baker. Micropor Mesopor Mater 33:281–289, 1999.
194. CA Bessel, DR Rolison. Stud Surf Sci Catal 98:114–115, 1995.
195. T Nyokong. J Chem Soc Dalton Trans 90:1359–1365, 1994.
196. G Shi, G Xue, W Hou, J Dong, G Wang. J Electroanal Chem 344:363–366, 1993.
197. RN de Guzman, YF Shen, BR Shaw, SL Suib, CL O'Young. Chem Mater 5:1395–1400, 1993.
198. O Schäf, H Ghobarkar, AC Steinbach, U Güth. Fresenius J Anal Chem 367:388–392, 2000.

199. NJ Turro, M Garcia-Garibay. In: V Ramamurthy, ed. Photochemistry in Organized Media. New York: VCH, 1991, pp 1–38.
200. S Bharathi, KLN Phani, J Joseph, S Pitchumani, D Jeyakumar, GP Rao. J Electroanal Chem 360:347–349, 1993.
201. LT Kubota, Y Gushikem, J Perez, AA Tanaka. Langmuir 11:1009–1013, 1995.
202. MD Baker, C Senaratne. Brit UK Patent No. GB 2,252,831 (1992).
203. MD Baker. Can Chem News 44:16–17, 1992.
204. MD Baker, C Senaratne. Can Patent No. CA 2,179,472 (1997).
205. MD Baker, C Senaratne. US Patents Nos. 5,733,437 and 5,730,857 (1998).
206. WW Buchberger, PR Haddad. J Chromatogr A 789:67–83, 1997.
207. P Mariaulle, F Sinapi, L Lamberts, A Walcarius. Electrochim Acta 46:3543–3553, 2001.
208. HH Girault. In: JO Bockris, ed. Modern Aspects of Electrochemistry, Vol. 25. New York: Plenum, 1993, pp 1–62.
209. F Reymond, D Fermin, HJ Lee, HH Girault. Electrochim Acta 45:2647–2662, 2000.
210. PA Jacobs, NI Jaeger, P Jiru, G Schultz-Ekloff, eds. Metal Microstructures in Zeolites: Preparation, Properties, Applications. Amsterdam: Elsevier, 1982.
211. J Heinze. Angew Chem Int Ed Engl 30:1268–1288, 1993.
212. M Fleischmann, J Ghoroghchian, DR Rolison, S Pons. J Phys Chem 90:6392–6400, 1986.
213. DR Rolison, J Stemple. US Patent No. 5,282,936 (1994).
214. DR Rolison, J Stemple. US Patent No. 5,288,371 (1994).
215. DR Rolison, J Stemple. US Patent No. 5,296,106 (1994).
216. ML Hamlaoui, R Kherrat, M Marakchi, N Jaffrezic-Renault, A Walcarius. Mater Sci Eng C 21:25–28, 2002.
217. A Walcarius. Electroanalysis 13:701–718, 2001.
218. W Huang, Y Yan, C Wan, J Wang. Qinghua Daxue Xuebao Ziran Kexueban 40:70–73, 2000.
219. SM Kuznicki, JS Curran, X Yang. World Patent No. 9,832,695 (1998).
220. J Rocha, MW Anderson. Eur J Inorg Chem 5:801–818, 2000.
221. M Inagaki, H Nagura, T Murata, Y Harada. Jp Patent No. 11,204,143 (1999).
222. H Nemoto. Eur Patent No. 942,485 (1999).
223. S Kamiharashi, H Jinbo, K Naruse, S Fukuda. Jp Patent No. 63,019,765 (1988).
224. Fuji Electrochemical Co., Ltd. Jp Patent No. 59,224,071 (1984).
225. Hitachi Maxell, Ltd. Jap Patent No. 59,081,869 (1984).
226. JE Casey Jr, RF Chireau. US Patent No. 3,864,168 (1975).
227. Kamiharashi, K Naruse, H Jinbo. Jp Patent No. 62,168,349 (1987).
228. T Inoue, K Kobayashi, K Matsuo. Jp Patent No. 62,193,060 (1987).
229. V Gartstein, JB Camden. World Patent No. 9,960,654 (1999).
230. T Hatakezawa, T Hara, T Endo, K Hatta. Jp Patent No. 2001,155,790 (2001).
231. D Kalaiselvi, R Renuka. J Chem Technol Biotechnol 75:285–293, 2000.
232. AS Berchielli, RF Chireau. Ger Patent No. 2,938,523 (1980).
233. M Shelef. US Patent No. 6,117,581 (2000).
234. M Cruceanu, E Popovici, A Vasile. Rom Patent No. 78,511 (1982).
235. M Cruceanu, E Popovici, A Vasile. Rom Rev Chim 32:973–975, 1981.
236. A Vasile, E Popovici, M Cruceanu. Rom Rev Chim 47:847–851, 1996.
237. GJ Bratton, T Naylor, ACC Tseung. World Patent No. 9,852,243 (1998).
238. K Miwa, K Iwayama, H Fukui. Jp Patent No. 62,241,265 (1987).
239. M Lanz, G Calzaferri. J Photochem Photobiol A Chem 109:87–89, 1997.